ELSEVIER

Chemical Engineering Journal 140 (2008) 305–323

Chemical Engineering Journal

www.elsevier.com/locate/cej

Simulated moving bed reactor for isomerization and separation of *p*-xylene

Mirjana Minceva, Pedro Sá Gomes, Vera Meshko, Alírio E. Rodrigues *

Laboratory of Separation and Reaction Engineering, Associate Laboratory LSRE/LCM, Department of Chemical Engineering, Faculty of Engineering, University of Porto, Rua Dr. Roberto Frias, 4200-465 Porto, Portugal

Received 26 July 2007; received in revised form 18 September 2007; accepted 19 September 2007

Abstract

A novel simulated moving bed reactor (SMBR) application for *p*-xylene production, which combines xylene isomerization and selective adsorption operating in liquid phase, at temperatures between 453 and 573 K is proposed. The SMBR unit configuration and principle of operation are explained. Experimentally determined xylenes adsorption equilibrium and kinetics parameters are used in the description of the xylene adsorption step. The reaction kinetics reported in the literature is used in the modelling of a fixed bed isomerization reactor. The equivalent true moving bed reactor (TMBR) modelling strategy is applied in modelling of the SMBR unit for *p*-xylene production. The steady state model assumes axial dispersion, coupled external and internal mass transfer resistances, and multicomponent Langmuir isotherms. The influence of the switching time, operating temperature and length of the reactors on process performance is presented for two different feed compositions: (A) xylenes composition is the same as in the feed used in a PAREX unit; (B) xylenes composition is the same as in the raffinate stream from the PAREX unit (both cases calculated on ethylbenzene and desorbent free basis).

Keywords: Multifunctional reactor; Isomerization; *p*-Xylene; Process integration; Simulation

1. Introduction

The multifunctional reactor concept that combines reaction and separation within a single unit has been the subject of considerable attention in both university and industrial research [1]. Various theoretical works analyse the thermodynamic benefits of multifunctional reactors [2–4] or develop complete process structures [5]. Generalized and well-structured concepts have to be examined in the light of the real chemical systems in order to back-up the existing methodologies with practical features [6].

There is a general agreement that the integration of reaction and separation is a useful and powerful tool in chemical reaction engineering. However, the number of industrial applications is still relatively low and the main reasons are [7]: (i) it is often difficult to identify processes that need improvement by reactive separation; (ii) it is difficult to develop and design continuous counter current reactive separations because of their complex nature and the larger amount of kinetic data and physical parameters that are required; and (iii) the development of a reactive separation process is expensive and risky.

Integration of reaction and separation steps in one single unit has the obvious economical advantage of reducing the cost of unit operations for downstream purification steps. Besides reactive distillation, reactive extraction or membrane reactors, the combination of (bio) chemical reaction with simulated moving bed (SMB) chromatographic separator has been subject of considerable attention in the last 10 years. This integrated reaction-separation technology adopts the name of simulated moving bed reactor (SMBR). The first application of SMBR in zeolite catalysed alkylation reaction was patented by Zabrinsky and Anderson in 1977 [8]. One of the reasons for the recent growing interest in SMBR is the success in SMB industrialization and its potential for the use as integrated reactor-separator.

Fig. 1a shows a scheme of an SMBR and the principle of its operation. The SMBR consists of a set of packed columns, of uniform cross section and length L_c, interconnected in a closed circuit. The columns are packed with a solid, which acts as both adsorbent and catalyst or a mixture of both. There are two inlet streams (feed and eluent/desorbent) and two outlet streams (extract and raffinate). Let us consider a reaction $A \rightarrow B + C$. The reactant A is used as feed, product B, which is more strongly adsorbed component in the solid, is collected in the extract. The raffinate port collects the C enriched product. At regular time intervals, called switching time t^*, the inlet and outlet ports are

* Corresponding author. Tel.: +351 22 5081671; fax: +351 22 5081674.
E-mail address: arodrig@fe.up.pt (A.E. Rodrigues).

1385-8947/$ – see front matter © 2007 Elsevier B.V. All rights reserved.
doi:10.1016/j.cej.2007.09.033

Nomenclature

A	reactor (adsorber) cross-section area (m^2)
c	fluid concentration (kg/m^3)
$\bar{c}_p$	average pore concentrations (kg/m^3)
d_c	diameter of the column (m)
D_e	effective diffusivity (m^2/s)
DE	*p*-xylene deviation from equilibrium (%)
D_L	axial dispersion coefficient (m^2/s)
D_m	molecular diffusivity (m^2/s)
D_p	pore diffusivity (m^2/s)
E_l	activation energy of reaction l (J/mol)
ΔG°	standard Gibbs energy of reaction (J/mol)
ΔH°	standard enthalpy of reaction (J/mol)
ΔH_f°	standard molar enthalpy (heat) of formation (J/mol)
k_L	global mass transfer coefficient (m/s)
k_n	kinetic constants for n reaction ($m^3/s_{kg\ catalyst}$)
K	adsorption equilibrium constant (m^3/kg)
KMP, KMO, KOP	equilibrium reaction constants for *m*-xylene to *p*-xylene, *m*-xylene to oxylene and *o*-xylene to *p*-xylene reactions, respectively
L	length of the column (m)
LWHSV	liquid weight hourly space velocity ($Q\rho l/m_{cat}$) ($kg/(kg_{catalyst}\ h)$)
m_{cat}	mass of catalyst (kg)
P	pressure (Pa)
Pe	Peclet number
PR	raffinate productivity ($kg/h\ m^3$)
PUR	raffinate purity (%)
PUX	extract purity (%)
q	adsorbed phase concentration in equilibrium with c_p (kg/kg)
Q	flow rate (m^3/s)
Q_m	saturation adsorption capacity (kg/kg)
r_p	particle radius (m)
R	rate of the chemical reaction (s^{-1})
R_g	gas constant (J/(mol K))
Re_p	Reynolds number relative to particle, velocity
S°	standard molar entropy (J/mol)
ΔS°	standard entropy of reaction (J/mol)
Sc	Schmidt number
SC	desorbent consumption (m^3/kg)
Sh_p	Sherwood number relative to particle
t	time variable (s)
T	temperature (K)
T_{ref}	reference temperature (K)
u_s	solid velocity (m/s)
v	interstitial liquid velocity (m/s)
z	axial coordinate (m)

Greek letters

γ	ratio between the liquid and solid interstitial velocity
ε	bed porosity
ε_p	particle porosity
μ	liquid viscosity (kg/(m s))
ρ_l	average liquid density (kg/m^3)
ρ_p	particle density (kg/m^3)
τ	tortuosity

Subscripts and superscripts

E, X, D, F, R	eluent, desorbent, extract, feed and raffinate, respectively.
i	number of components ($i = p$x, mx, ox, desorbent)
j	number of column ($j = 1, 2, \ldots, N$)
l	number of reaction ($l = 1, -1, 2, -2, 3, -3$)

switched in the direction of fluid flow for one column. A cycle is completed when the number of switches is equal to the number of columns. In this way, the counter current motion of the solid is simulated with velocity $u_s = L_c/t^*$.

The relative motion of the chemical species in an SMBR can be easily understood by considering an equivalent true moving bed reactor (TMBR). In the TMBR (see Fig. 1b) the position of the inlet and outlet streams is kept unchanged. The solid really moves in the opposite direction to the fluid flow. According to the position of the inlet and outlet stream the unit can be divided in four zones. In zone 1, placed between the eluent and extract nodes, the adsorbent (and/or catalyst) is regenerated by removing the more strongly adsorbed product (*B*) from the adsorbent (and/or catalyst). The adsorbent (and/or catalyst) from the beginning of this zone is recycled to zone 4 in form of clean adsorbent. In zone 2, between the extract and feed node, the reaction is taking place and products (*B* and *C*) are formed. The less adsorbed product (*C*) is desorbed and transported with the liquid in direction of the raffinate port. The more strongly adsorbed product *B* is adsorbed and transported with the solid phase to the extract port. Zone 3 is between the feed and raffinate node. The task of this zone is the same as zone 2, the reaction goes on and the products are formed, component *B* is retained and carried out with the adsorbent and component *C* is collected in the raffinate. In zone 4, placed between the raffinate and eluent/desorbent node, the eluent/desorbent is regenerated before being recycled to zone 1. The component *C* is adsorbed and transported back to the zone 3 with the solid phase.

The SMBR technology is usually considered for: (i) reversible reactions where the conversion is limited by the chemical equilibrium; in this case the removal of products as they are formed allows achieving conversions well beyond equilibrium values; (ii) reactions in series or in parallel, it may be possible the selective separation of desired intermediate species and (iii) when a reaction product has an inhibiting or poisoning effects, its removal from the reaction medium also promotes enhanced yield.

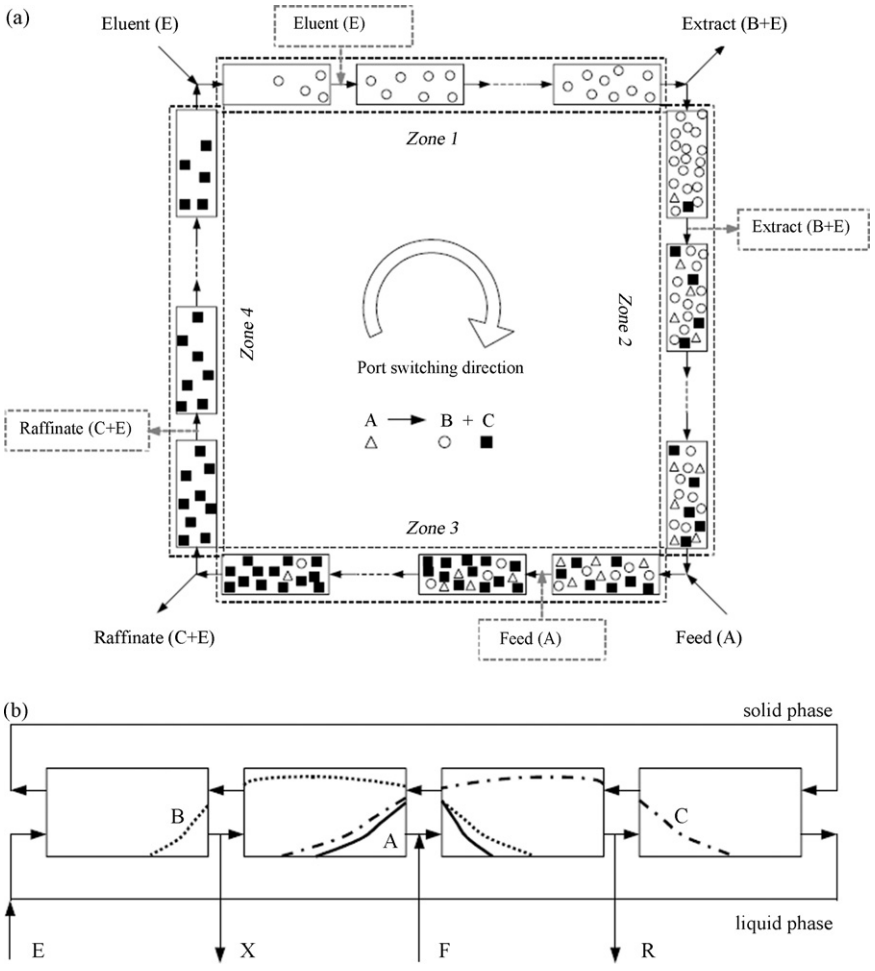

Fig. 1. Schematic diagram of (a) SMBR and (b) TMBR for reaction $A \rightarrow B + C$.

Regarding to the adsorbent and catalyst, there are two possible scenarios in the SMBR: (i) adsorbent and catalyst are two different materials; or (ii) catalyst and adsorbent are present in the same pellet. For most of the applications developed up to the mid 1990s, catalyst and adsorbent are essentially different materials, which may be mixed or arranged in alternate columns [9].

Another important aspect when considering the coupling of reaction and separation are the operating conditions used in both steps. If reaction and separation occur at different temperatures the SMBR technology is not applicable since the temperature gradients cannot be conveniently handled within the unit. Mazzotti et al. [10] investigated the esterification of acetic acid in an SMBR as a model reaction for which these effects are overcome.

Depending on the reactive system some interesting arrangements of the general SMBR setup can be found in the literature. If the less adsorbed product (component C in Fig. 1) is not adsorbed, the recycling of the eluent is not possible; therefore zone 4 can be eliminated [11]. On other hand, if, for the regeneration of the solid, a change of the operating conditions (temperature, pressure or type of eluent or desorbent) has to be applied, it would be more convenient to decouple zone 1 from the central unit [12]. For highly exothermic gas phase reactions it can be advantageous to use an alternative rearrangement of the purely catalytic and purely adsorptive columns in order to have better control of the internal temperature profiles [13]. Also, for reaction of type $A \leftrightarrow B$, Hashimoto and co-workers [9] used alternatively rearrangement of the columns, separating the columns where the reaction and separation takes place. A summary of the SMBR applications is presented in Table 1.

The selection of the operating parameters such as the length and number of columns, switching time, and liquid flow rates in different sections is not straightforward in an SMBR. In most cases, conflicting requirements and constraints govern the optimal choice of the decision (operating or design) variables [14]. The design and optimization of an SMBR are essential in evaluation of the process feasibility at industrial scale [15]. The design and optimization of chromatographic reactors of simulated moving bed type has been subject of several publications [14–24]. The design of an SMBR will define geometric and operating parameters that should lead not only to product separation, but also to high reactant conversions. Moreover, the amount of catalyst becomes an additional degree of freedom to the optimisation problem.

Design procedures based on equilibrium theory were applied to the separation of the reaction products in a non-reactive SMB [25]. The region of complete separation of products (separation triangle), was spanned by consecutive simulation

Table 1
Applications of simulated moving bed reactor technology

Reaction	Catalyst/enzyme	Phase	References
Isomerization of glucose $A \leftrightarrow B$	Isomerase + adsorbent	Liquid	[9]
Inversion of sucrose $A \rightarrow B + C$	Invertase	Liquid	[15,30–32]
Synthesis of dextran from sucrose	dextranosucrase	Liquid	[33]
Conversion of glucose to glucose-6-phosphate $A \leftrightarrow B$	Coenzyme ATP	Liquid	[34]
Hydrogenation of 1,3,5-trimethyl benzene $A \leftrightarrow B$	Pt on alumina	Gas	[35]
Methanol synthesis from syngas $A + B \leftrightarrow C$	Metal catalysts	Gas	[36]
Oxidative coupling of methane $2A + 1/2B \rightarrow C + D$; $2A + B \rightarrow E + 2D$; $A + 3/2B \rightarrow F + 2D$; $A + 2B \rightarrow G + 2D$	Sm_2O_3 + activated charcoal adsorbent $YBa_2Zr_3O_{9.5}$ + activated charcoal	Gas	[13,37–39]
Saccharification of modified starch $A \rightarrow B + C$	Maltogenase	Liquid	[12]
Hydrolysis of lactose $A \leftrightarrow B + C$	Lactase	Liquid	[40]
Esterification of acetic acid with β-phenethyl alcohol $A + B \leftrightarrow C + D$	Ion-exchange resin	Liquid	[41]
Esterification of acetic acid with ethanol $A + B \leftrightarrow C + D$	Amberlyst 15	Liquid	[10,25]
Synthesis of bisphenol A from acetone and phenol $A + 2B \leftrightarrow C + D$	Amberlyst 31	Liquid	[11]
Production of lactosucrose from sucrose and lactose	β-Fructofuranosidase	Liquid	[42]
Esterification of acetic acid with methanol $A + B \leftrightarrow C + D$	Amberlyst 15	Liquid	[43–45]
Synthesis MTBE from *tert*-butyl alcohol and methanol $A + B \leftrightarrow C + D + E$	Amberlyst 15	Liquid	[46]
Diethylacetal synthesis from ethanol and acetaldehyde $2A + B \leftrightarrow C + D$	Amberlyst 15 Amberlyst 18	Liquid	[20,47]
Isomerization of 2-methylpentane to 2,2 dimethylbutane	MFI zeolite	Gas	[48]
Esterification of acrylic acid with methanol	Amberlyst 15	Liquid	[49]
Selective catalytic reduction (SCR) of NO_x with NH_3	Zeolite NO_xCAT^{TM} ETZ	Gas	[50]

using a detailed model that included the reaction kinetics [26]. Dünnebier et al. [24], presented a novel optimisation and design strategy for an SMBR based on mathematical optimisation, a rigorous process model and a detailed cost function. The results are restricted to an existing SMBR unit geometry. The algorithm for design of physical configuration of a new unit was proposed by Biressi et al. [27] and extended by Azevedo and Rodrigues [15], by inclusion of the reaction conversion as a design constraint and a detailed model for the SMBR process. Recently, the use of the multiobjective optimization of SMBR was proposed [14,28,29].

The main objective of this work is to present a novel simulated moving bed reactor for *p*-xylene production, which combines xylene isomerization and selective adsorption, operating in liquid phase at temperatures between 453 and 573 K. The article is arranged as follows: (i) the current industrial process for *p*-xylene production will be briefly described; (ii) the xylene isomerization will be reviewed; (iii) the novel SMBR application to *p*-xylene production is described; (iv) simulation of SMBR is addressed in order to find appropriate operating conditions.

2. Xylenes separation/isomerization loop

The C_8 aromatics fraction in a refinery consists mainly of four xylene isomers, i.e., *o*-, *m*-, and *p*-xylene and ethylbenzene; *p*-xylene is the one with major industrial importance since it is widely used in the manufacture of synthetic fibres. However, the equilibrium amount of the *p*-xylene obtained in the catalytic reformers is only 24% and therefore is not sufficient to cover industrial demand. This problem is overcome in industry by re-isomerization of the *p*-xylene depleted stream. A typical xylene separation/isomerization loop used in the industrial *p*-xylene production is presented in Fig. 2. The loop consists of an SMB unit and xylene isomerization reactor. In the SMB unit the mixed xylenes stream is separated by selective adsorption in two streams: *p*-xylene reach stream-extract and *p*-xylene depleted stream-raffinate. The *p*-xylene reach stream is collected as final product. The *p*-xylene depleted mixture free of desorbent (toluene in Fig. 2, although *p*-diethylbenzene is often used as desorbent) is sent to the xylene isomerization unit, where isomerization to equilibrium mixture of xylenes is carried out. The

Table 2
Operating conditions of xylene separation/isomerization processes

Process	Phase	T (°C)	P (bar)	Adsorbent/catalyst
SMB p-xylene separation	Liquid	170–185	8–9	Ba and/or K exchanged zeolite X and Y
Xylene isomerization	Vapour (under H_2 flow)	380–480	10–28	Dual-functional Pt catalyst ZSM-5 zeolites

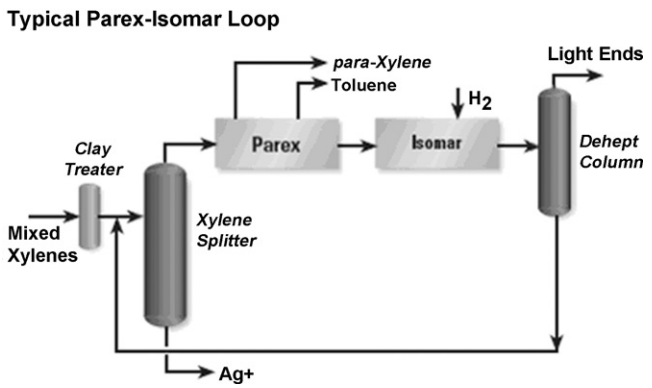

Fig. 2. Schematic presentation of separation/isomerization loop ("Parex Process", 2006, UOP-Honeywell, USA).

xylene equilibrium mixture is then recycled to the feed of the p-xylene separation unit-SMB. Operating conditions of industrial an SMB p-xylene separation processes and xylene isomerization are shown in Table 2.

Coupling of xylene separation and reaction (isomerization) step in one unit under operating conditions given in Table 2 is not possible, because of different operating temperatures and different phases. The need of the hydrogen flow in the xylene isomerization for catalyst protection from coking is an additional difficulty. Therefore we propose a novel SMBR unit for p-xylene production by isomerization of xylene mixture free of ethylbenzene operating in liquid phase.

3. Xylene isomerization kinetics and adsorption data

The type of catalyst used in the xylene isomerization depends on the presence of ethylbenzene in the xylene mixture. When ethylbenzene is present, bi-functional noble metal acid catalysts are used and the isomerization reaction is carried out under hydrogen pressure. Acid catalysts are used for isomerization of xylene mixtures free of ethylbenzene. There are two options for ethylbenzene conversion: inclusion of the ethylbenzene in the xylene isomerization reaction and dealkylation of ethylbenzene into benzene. Pure xylene isomerization on acid catalysts is accomplished by several other conversion reactions, e.g. dealkylation and transalkylation. It is known that there is strong increase in the ratio between the rates of xylene isomerization and xylene disproportionation when zeolite pore size becomes smaller [51]. A survey of xylenes isomerization research, considering a triangular reaction scheme, is shown in Table 3, where it can be observed that most of the isomerization processes are carried out in the gas phase.

3.1. Modelling reaction kinetics of xylene isomerization

In this work the xylene izomerization in liquid phase in absence of ethylbenzene is considered and literature data presented by Cappellazzo et al. [56] are used. Cappellazzo and co-workers investigated the kinetics of xylenes isomerization in liquid phase over a ZSM-5 catalyst at temperature between 523 and 573 K in a fixed bed catalytic reactor. They proposed the triangular reaction scheme:

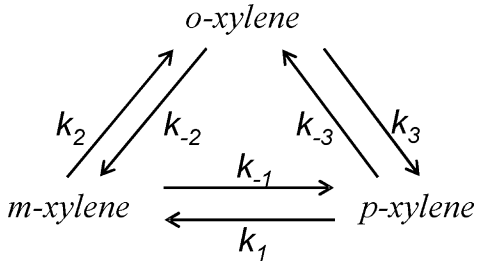

Assuming a single site surface rate controlled Langmuir–Hinshelwood kinetics, the rate of reactions, r_l, are: $r_1 = (k_1 c_{px} - k_{-1} c_{mx})/D$, $r_2 = (k_2 c_{mx} - k_{-2} c_{ox})/D$ and $r_3 = (k_3 c_{ox} - k_{-3} c_{px})/D$, where c_i is the concentration of the isomer i ($i = o - x(1)$, $m - x(2)$ and $p - x(3)$), K_i is the adsorption equilibrium constant for ith isomer, k_l is the kinetic constants for l reaction and $D = 1 + K_{px} c_{px} + K_{mx} c_{mx} + K_{ox} c_{ox}$.

In absence of mass transfer limitations the rates of consumption of o-, m-and p-xylene are:

$$R_1 = (k_3 + k_{-2}) c_{p1} - k_2 c_{p2} - k_{-3} c_{p3} \quad (1)$$

$$R_2 = (k_2 + k_{-1}) c_{p2} - k_1 c_{p3} - k_{-2} c_{p1} \quad (2)$$

$$R_3 = (k_1 + k_{-3}) c_{p3} - k_{-1} c_{p2} - k_3 c_{p1} \quad (3)$$

Cappellazzo et al. [56] calculated the reaction kinetic constants k_l by fitting of the xylene isomerization experimental data obtained in fixed bed catalytic reactor at 523, 553 and 573 K by assuming $D = 1$ (elimination the adsorption constants) and introducing the equilibrium reaction constants $K_{MP} = k_{-1}/k_1$, $K_{MO} = k_2/k_{-2}$ and $K_{OP} = k_3/k_{-3}$ (elimination of three kinetic constants) where $K_{MP} = (c_{px}/c_{mx})_{eq}$, $K_{MO} = (c_{ox}/c_{mx})_{eq}$, $K_{OP} = (c_{px}/c_{ox})_{eq}$ are the equilibrium constants for m-xylene to p-xylene, m-xylene to o-xylene and o-xylene to p-xylene reactions, respectively.

Reaction equilibrium constants (K_{MP}, K_{MO}, K_{OP}) at 298.15 K were calculated from the Gibbs free energy $\Delta G^\circ = -RT \ln(K)$, where $\Delta G^\circ = \Delta H^\circ - T\Delta S^\circ$. The standard enthalpy and entropy of reaction: $\Delta H^\circ = \sum \Delta H^\circ_{products} - \sum \Delta H^\circ_{reactants}$ and $\Delta S^\circ = \sum \Delta S^\circ_{products} - \sum \Delta S^\circ_{reactants}$ were computed from standard thermodynamic data: molar enthalpy (heat) of formation (ΔH°_f) and molar entropy (S°) presented in Table 4.

Table 3
Survey of xylene isomerization investigations, considering a triangular reaction scheme (a) in gas phase and (b) liquid phase

System	Type of reaction	Application	References
(a) Xylene/zeolite USY	Xylene isomerization	Experimental, kinetics study and modelling	[52,53]
(a) Xylene/ZSM-5	Isomerization	Modeling and kinetics	[54]
(a) Xylene/ZSM-5	Xylene isomerization	Test of catalyst, mechanism of reaction	[55]
(b) Xylene/ZSM-5	Isomerization	Modeling	[56]
(a) Xylene/SiANi-4	Isomerization	Mechanism of reaction	[57]
(a) Xylene/AlANi-4	Isomerization	Kinetics	[58]
(a) C_8 aromatics/Pt-zeolite	Isomerization	Modeling	[59]
(b) Xylene/mordenite xylene/Hmordenite	Xylene isomerization	Testing of catalyst and/or kinetics	[60,61]

Table 4
Standard thermodynamic data

	p-Xylene	*o*-Xylene	*m*-Xylene
ΔH_f° (kJ/mol)	−24.4	−24.45	−25.30
S° (J/mol)	249.52	247.06	253.05

The temperature dependence of the reaction rate was determined from Arrhenius equation: $k_l = k_l\ (T_{ref}) \exp[-E_l/R\ (1/T - 1/T_{ref})]$, $l = 1, -1, 2, -2, 3, -3$ where T_{ref} is the reference temperature ($T_{ref} = 553$ K). The values of reaction rate constants obtained by Cappellazzo et al. [56] at 553 K are $k_{-1} = 1.06 \times 10^{-6}$, $k_{-2} = 0.64 \times 10^{-6}$ and $k_{-3} = 0.58 \times 10^{-6}$ m^3/(s kg) and activation energies $E_{-2(ox \to mx)} = 98.74$, $E_{-1(mx \to px)} = 135.98$ and $E_{-3(px \to ox)} = 158.15$ kJ/mol for a liquid phase xylene isomerization on ZSM-5 catalyst. The reaction rate constants in temperature range between 453 and 573 K are presented in Table 5.

The kinetic of isomerization of xylene mixture containing 27.5 wt% *o*-xylene, 60.4 wt% *m*-xylene and 12.1 wt% *p*-xylene was simulated and the equilibrium composition at different temperatures between 453 and 573 K is presented in Table 6.

A more detailed fixed bed catalytic reactor model was developed, including external mass transfer resistance, axial dispersion, diffusion inside catalyst pellet, coupled with chemical reaction within an individual catalyst pellet, and is presented in Appendix A. Nevertheless, the detailed models normally requires longer computation time when applied for the simulation of more complex systems, as for example the SMBR. Therefore, it was also studied a simplified model by coupling the external (film mass transfer) and internal mass transfer (pore diffusion) in a single mass transfer step. The mass transfer from the bulk liquid phase to the zeolite particle was presented with a linear driving force (LDF) model and total mass transfer coefficient [62] see Appendix A.

Both models give good prediction of the steady state xylenes (fixed bed reactor) outlet composition calculated by Cappellazzo et al. [56]. Nevertheless, the lumped model was selected and used in the modelling of the SMBR unit for *p*-xylene production.

Table 5
Reaction rate constants at different temperatures

T (K)	$k_l \times 10^8$ (m^3/s kg)					
	k_{-1}	k_1	k_{-2}	k_2	k_{-3}	k_3
453	0.15	0.30	0.56	0.22	0.03	0.04
493	2.89	5.49	4.66	1.84	0.88	1.17
533	34.72	65.28	28.33	11.39	15.83	21.11
553	105.56	196.39	63.61	25.83	57.78	76.94
573	296.39	547.50	134.72	54.72	191.94	255.28

Table 6
Equilibrium xylene composition at different temperatures

T (K)	*o*-x (wt%)	*m*-x (wt%)	*p*-x (wt%)
453	22.23	54.99	22.77
493	22.46	54.51	23.03
533	22.65	54.11	23.24
553	22.74	53.93	23.33
573	22.82	53.76	23.42

3.2. Xylene adsorption

The *p*-xylene and *o*-xylene adsorption isotherm on Ba exchanged Faujasite type of adsorbent were measured experimentally in the temperature range between 303 and 453 K [63]. According to the literature, the *m*-xylene isotherm is very similar to that of *o*-xylene. Therefore, in this study the *m*-xylene adsorption isotherm is considered identical to the one of *o*-xylene.

The xylenes adsorption equilibrium is presented with the Langmuir model. The experimental determined Langmuir isotherm parameters at temperature between 303 and 453 K were extrapolated to the temperature of 573 K.

The desorbent is such that the adsorption equilibrium is that of *p*-diethylbenzene on KY zeolite at 453 K provided by Neves [64]. The desorbent isotherm parameters on higher temperatures were calculated relatively to the *p*-xylene adsorption isotherm parameters. The ratio $K_{desorbent}/K_{p\text{-x}}$ and the ratio $Q_{m\,desorbent}/Q_{mp\text{-x}}$ in the Langmuir isotherm, calculated at 453 K was used to calculated the desorbent Langmuir parameters at each temperature:

$$K_{desorbent}(T) = 1.21364 K_{p\text{-x}}(T) \quad (4)$$

$$Q_{m\,desorbent}(T) = 0.82655 Q_{mp\text{-x}}(T) \quad (5)$$

The xylenes and desorbent Langmuir isotherm parameters at different temperatures are presented in Table 7.

Table 7
Xylenes isotherm parameters at different temperatures

Component	Temperatute							
	453 K		493 K		533 K		573 K	
	K[a]	Q_m[b]	K	Q_m	K	Q_m	K	Q_m
p-Xylene	1.941	0.1024	1.215	0.0977	0.7570	0.0957	0.504	0.0940
o-Xylene	0.888	0.0917	0.649	0.0909	0.501	0.0900	0.401	0.0893

[a] (m^3/kg).
[b] (kg/kg).

4. Novel SMBR application for *p*-xylene production

The configuration of the novel SMBR for *p*-xylene production is inspired on the scheme proposed by Hashimoto [9] presented in Fig. 3, at time 0 and at switching time (t^*); in this reference case there are two reactors and three adsorbers in zone 3.

The SMBR consist the four zones as the classical SMBR scheme (see Fig. 1a). The characteristics of this configuration are: (i) reactors just in zone 3; (ii) zone 3 starts with adsorber and finishes with adsorber; (iii) the reactors switch in direction of the liquid flow together with the inlet (feed and desorbent) and outlet (extract and raffinate) streams; therefore the reactors are fixed relatively to the inlet and outlet streams; and (iv) the feed enters first in the adsorber (each switch time in the next adsorber in direction of the liquid flow).

This SMBR process for *p*-xylene production will be investigated through numerical simulation, in order to identify the governing design parameters.

Two different feed compositions were used in the simulation study (see Table 8):

- *Feed A* composition (calculated on ethylbenzene free basis) is that of the feed used in the PAREX unit. The weight percent *p*-xylene is higher than the one predicted from the reaction equilibrium (see Table 6).
- *Feed B* composition is that of the raffinate stream from the PAREX unit (the composition is calculated on ethylbenzene and desorbent free basis). The weight percent *p*-xylene is much lower than the one predicted from the reaction equilibrium (see Table 6).

Table 8
Feed composition of SMBR for *p*-xylene production

Component	Feed composition (wt%)	
	Feed A	Feed B
p-Xylene	27.44	0.68
m-Xylene	57.79	79.11
o-Xylene	14.77	20.21

The SMBR unit used in the simulation study has the following configuration: zone 1 (between the desorbent and extract node), six adsorbent columns, zone 2 (between the extract and feed node), nine adsorbent columns, zone 3 (between the feed and raffinate node), six adsorbers and five reactors, starting with adsorber and finishing with adsorber and zone 4 (between the raffinate and desorbent node), three columns.

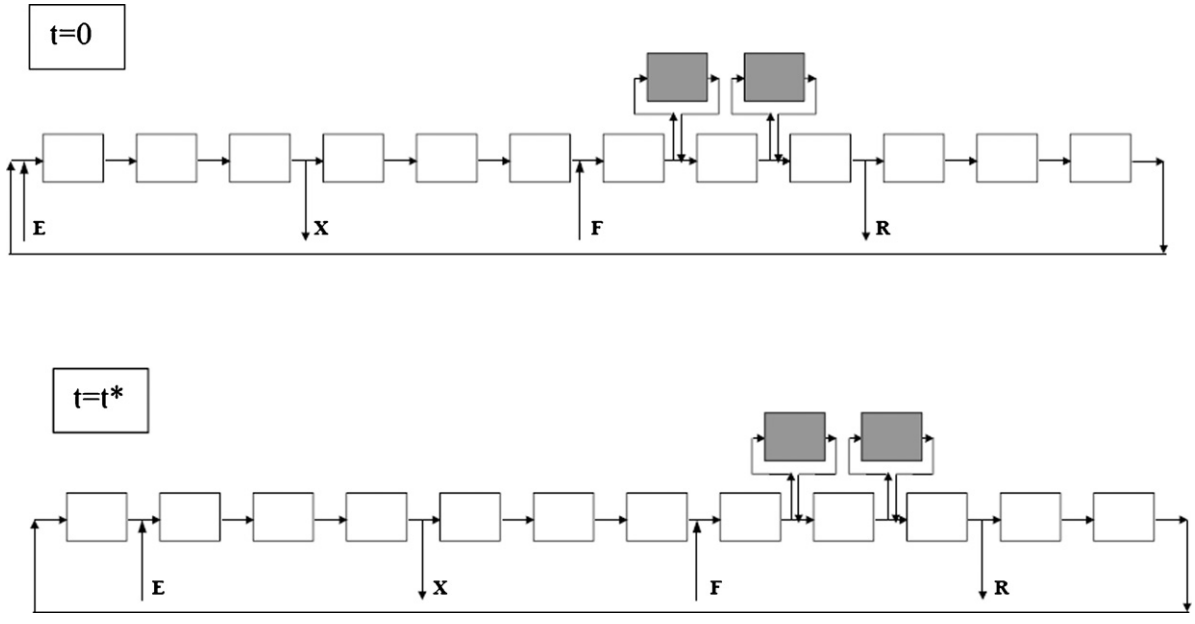

Fig. 3. SMBR configuration for *p*-xylene production with two reactors and three adsorbers in zone 3 (reference case), (□) adsorber and (■) reactor.

Table 9
SMBR operating conditions and model parameters

SMBR unit geometry
$L_c = 1.135$ m
$d_c = 4.12$ m
$V_c = 15.13\ m^3$
Number of columns: 29
Configuration: 6-9-(6 + 5)-3
Operating conditions
$T = 453$ K
$t^* = 1.15$ min
$Q_F^* = 62.29\ m^3/h$
$Q_X^* = 96.44\ m^3/h$
$Q_R^* = 197.83\ m^3/h$
$Q_D^* = 231.99\ m^3/h$
$Q_I^* = 674.47\ m^3/h$
Model parameters
$Pe_j = \frac{v_j L_j}{D_{Lj}} = 500$
$\varepsilon = 0.39$
$\varepsilon_p = 0.37$
$d_p = 0.062$ cm
$\rho_{\rho(ads)} = 1.48\ g/cm^3$
$\rho_{\rho(cat)} = 0.930\ g/cm^3$
$k_{L(p\text{-x},\ m\text{-x},\ o\text{-x})} = 5.02\ min^{-1}$
$k_{L(p\text{-DEB})} = 4.25\ min^{-1}$

The SMBR operating conditions and model parameters at 453 K are presented in Table 9.

5. Modelling of SMBR for *p*-xylene production

Two modelling strategies can be applied in the modelling of the SMBR: true moving bed reactor and simulated moving bed reactor model. Both strategies convey essentially the same information at steady state, when large number of columns per section is present. In the SMBR, the reactor columns switch together with the inlet and outlet streams the catalyst actually does not move relatively to the liquid phase. Therefore, the interstitial liquid and solid velocity in the reactors and adsorbers in the equivalent TMBR are:

- In the adsorbers:

$$\text{liquid velocity}: v_{TMBR} = v_{SMBR} - u_s,$$

$$\text{solid velocity}: u_s = \frac{L_c}{t^*}$$

- In the reactors:

$$\text{liquid velocity}: v_{TMBR} = v_{SMBR}, \quad \text{solid velocity}: u_s = 0$$

The equivalent TMBR to the SMBR configuration presented in Fig. 3 (reference case) is given in Fig. 4.

SMBR modelling strategy is more precise than the TMBR model, since it represents the actual physical equipment operation. However, due to the higher computational effort required in the solution for SMBR strategy, especially when a large number of columns are involved, the TMBR strategy has been considered in the SMBR performance prediction. The proposed mathematical model is based on following assumptions: steady state operation; the feed is free of ethylbenzene; the desorbent does not react with the xylenes; the reaction of isomerization takes place just in zone 3; mass transfer coefficients and physicochemical parameters are independent of mixture composition; bed void fraction, radius and porosity of the adsorbent and catalyst are equal; the apparent density of the adsorbent and catalyst are different; negligible thermal effects, isothermal operation; negligible pressure drop and constant interstitial fluid velocity along each section.

The steady state TMBR mathematical model considers axial dispersion flow for the liquid phase and plug flow for the solid phase, linear driving force (LDF) for the intraparticle mass transfer rate and multicomponent adsorption equilibria for the adsorption columns and triangular reaction scheme for xylene isomerization for reaction columns. Model equations are:

Bulk fluid mass balance for component i in zone j:

$$D_{Lj}\frac{d^2c_{ij}}{dz^2} = v_j\frac{dc_{ij}}{dz} + \frac{1-\varepsilon}{\varepsilon}\frac{3}{r_p}k_{Li}(c_{ij} - \bar{c}_{pij})$$

$$i = 1, 2, 3\ (ox, mx, px)\ j = 1, 2, 3, 4 \qquad (6)$$

where c_{ij} and $\bar{c}_{pij}$ are the bulk and average particle concentrations in fluid phase of component i in zone j of the TMBR, respectively,

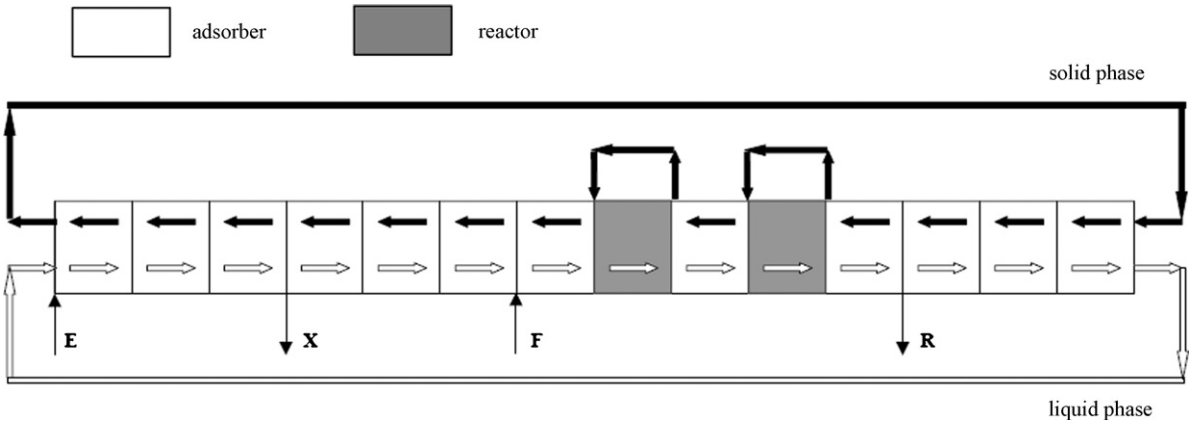

Fig. 4. Equivalent TMBR presentation of SMBR with 2 reactors and 3 adsorbers in zone 3 (reference case in Fig. 3).

k_{Li} is the global mass transfer coefficient of component i, ε is the bulk porosity, D_{Lj} and v_j are the axial dispersion coefficient and the interstitial velocity in zone j, respectively, r_p is the particle radius, z is the axial coordinate.

Adsorbent particle mass balance to component i in zone j:

$$0 = u_s \left(\varepsilon_p \frac{d\bar{c}_{pij}}{dz} + \rho_{p(ads)} \frac{dq_{ij}}{dz} \right) + \frac{3}{r_p} k_{Li}(c_{ij} - \bar{c}_{pij}) \quad (7)$$

Multicomponent adsorption equilibrium isotherm:

$$q_{ij} = Q_{m_i} \frac{K_i \bar{c}_{pij}}{1 + \sum_{k=1}^{n} K_k \bar{c}_{pij}} \quad (8)$$

Catalyst particle mass balance for component i in zone 3:

$$0 = \frac{3}{r_p} k_{Li}(c_{ij} - \bar{c}_{pij}) + \rho_{p(cat)} R_{ij} \quad (9)$$

Rate of reaction:

$$R_{1j} = (k_3 + k_{-2})\bar{c}_{p1j} - k_2 \bar{c}_{p2j} - k_{-3}\bar{c}_{p3j} \quad (10a)$$

$$R_{2j} = (k_2 + k_{-1})\bar{c}_{p2j} - k_1 \bar{c}_{p3j} - k_{-2}\bar{c}_{p1j} \quad (10b)$$

$$R_{3j} = (k_1 + k_{-3})\bar{c}_{p3j} - k_{-1}\bar{c}_{p2j} - k_3 \bar{c}_{p1j} \quad (10c)$$

Boundary conditions

$$z = 0: \quad D_{Lj} \frac{dc_{ij}}{dz} = v_j (c_{ij} - c_{ij}^{in}) \quad (11a)$$

$$z = L: \quad \frac{dc_{ij}}{dz} = 0 \quad \text{for reactors} \quad (11b)$$

$$z = L: \quad \frac{dc_{ij}}{dz} = 0 \quad \text{and} \quad \bar{c}_{pij,Lj} = \bar{c}_{pij+2,0}$$

for adsorbers in section 3 (11c)

$$z = L: \quad \frac{dc_{ij}}{dz} = 0 \quad \text{and} \quad \bar{c}_{pij,Lj} = \bar{c}_{pij+1,0}$$

for adsorbers in the others sections (11d)

where q_{ij} is the adsorbed phase concentration of component i in section j in equilibrium with $\bar{c}_{pij}$, u_s is the solid velocity and ε_p is the particle porosity, ρ_p is the particle density (adsorbent

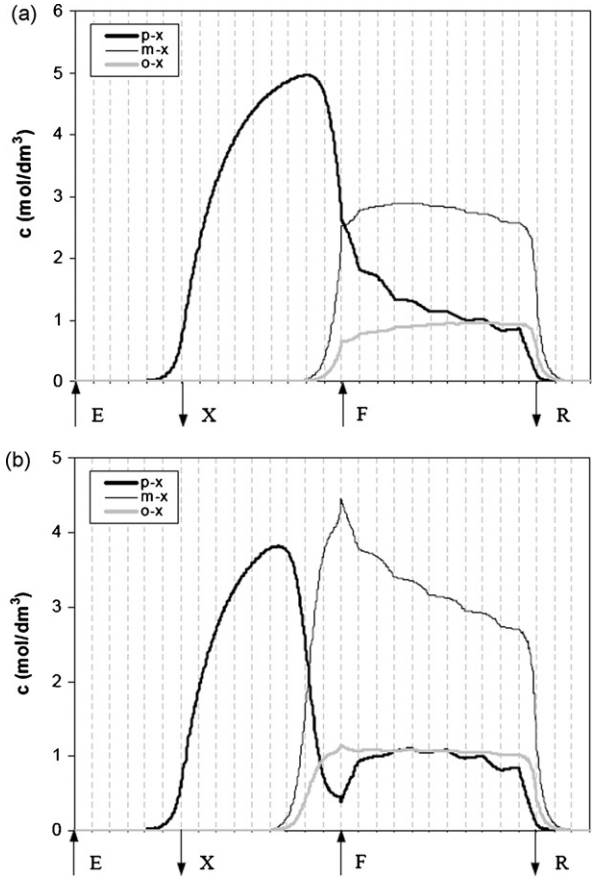

Fig. 5. Steady state concentration profiles in equivalent TMBR with (a) feed A and (b) feed B.

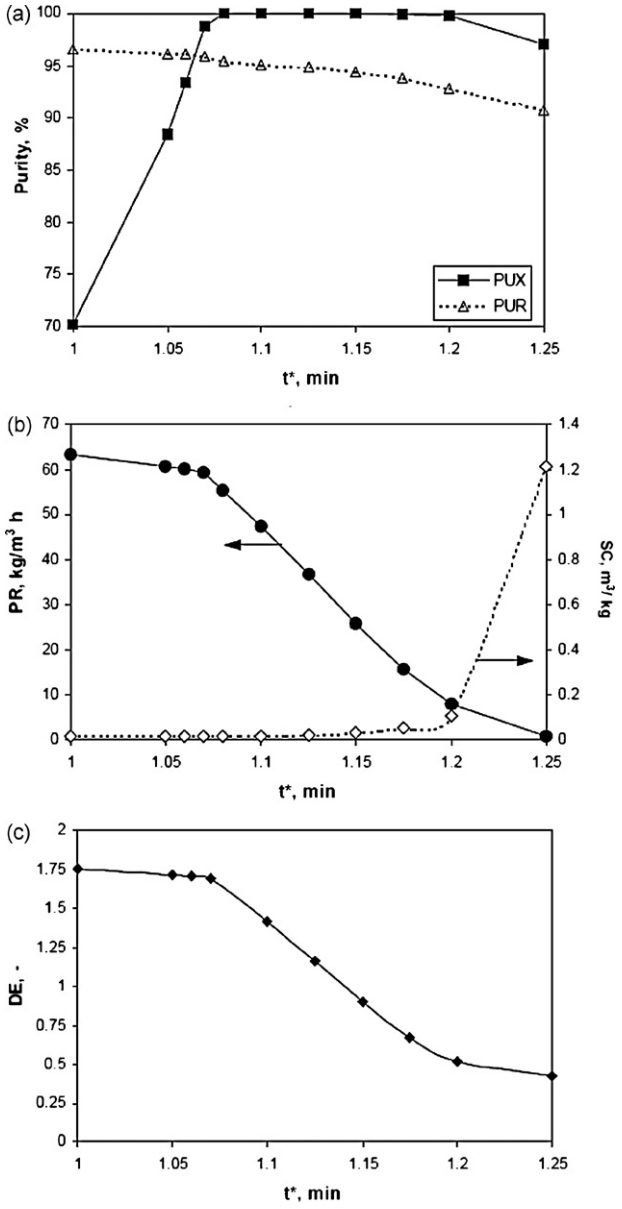

Fig. 6. Influence of the switching time for feed A on the (a) extract and raffinate purities; (b) *p*-xylene productivity and desorbent consumption; (c) *p*-xylene deviation from the equilibrium.

or calatyst), R is the rate of the chemical reaction relative to the average particle concentrations ($\bar{c}_{pij}$), Q_{mi} and K_i represent the saturation adsorption capacity and the equilibrium constant for component i, respectively.

Mass balances at the nodes of the inlet and outlet lines of the TMBR

- Desorbent node:

$$Q_4 + Q_D = Q_1 \tag{12a1}$$

$$c_{i,4}^{out} Q_4 + c_{i,D} Q_D = c_{i,1}^{in} Q_1 \tag{12a2}$$

- Extract node:

$$Q_1 - Q_X = Q_2 \tag{12b1}$$

$$c_{i,1}^{out} = c_{i,2}^{in} = c_{i,X} \tag{12b2}$$

- Feed node:

$$Q_2 + Q_F = Q_3 \tag{12c1}$$

$$c_{i,2}^{out} Q_2 + c_{i,F} Q_F = c_{i,3}^{in} Q_3 \tag{12c2}$$

- Raffinate node:

$$Q_3 - Q_R = Q_4 \tag{12d1}$$

$$c_{i,3}^{out} = c_{i,4}^{in} = c_{i,R} \tag{12d2}$$

In these equations, Q_j is the flow rate through zone j; Q_D is the desorbent flow rate, Q_F the feed flow rate, Q_X the extract flow rate and Q_R the raffinate flow rate. The fluid flow rates are related to the liquid-phase velocity, v_j, by $Q_j = \varepsilon A v_j$, where A is the zone (column) cross-section area.

The process performance was evaluated through the criteria:

- Extract purity (%):

$$\text{PUX} = \frac{c_{px,X}}{c_{ox,X} + c_{mx,X} + c_{px,X}} \times 100$$

- Raffinate purity (%):

$$\text{PUR} = \frac{c_{ox,R} + c_{mx,R}}{c_{ox,R} + c_{mx,R} + c_{px,R}} \times 100$$

- Desorbent consumption (m^3/kg):

$$\text{SC} = \frac{Q_D}{C_{px,X} Q_X}$$

- Productivity (kg/(h m^3))

$$\text{PR} = \frac{c_{px,X} Q_X}{V_{ads} + C_{cat}}$$

- p-Xylene deviation from equilibrium:

$$\text{DE} = \frac{Q_X c_{px,X} + Q_R c_{px,R}}{Q_F c_{px,eq}}$$

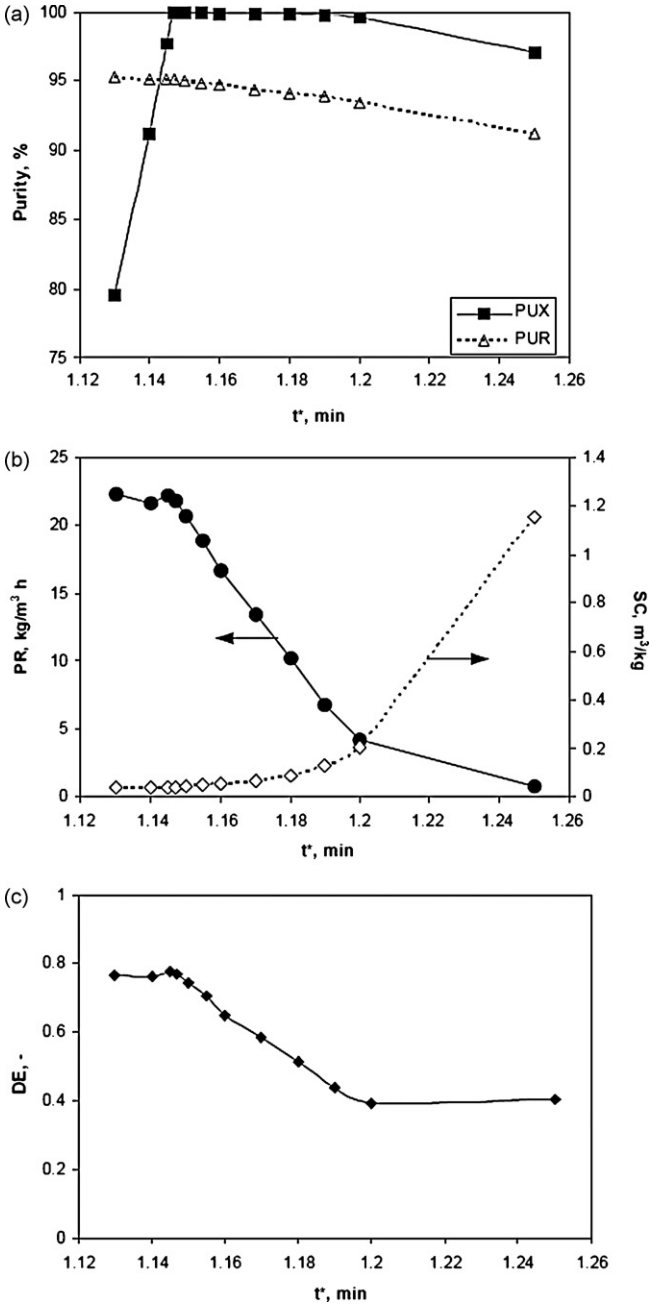

Fig. 7. Influence of the switching time for feed B on the (a) extract and raffinate purity; (b) p-xylene productivity and desorbent consumption; (c) p-xylene deviation from equilibrium.

where $c_{px,eq}$ is the p-xylene equilibrium composition. The p-xylene equilibrium composition at different temperatures between 453 and 573 K is presented in Table 6.

The model equations were solved with gPROMS ("gPROMS v2.2 User Guide", 2003), from Process System Enterprise, http://www.psenterprise.com. The mathematical model involves a system of partial and algebraic equations (PDAEs). A third order orthogonal collocation in finite elements method (OCFEM) was used in the discretization of axial and radial domain. Twenty-three elements, with two collocation points in each element, were used in discretisation of the axial and radial

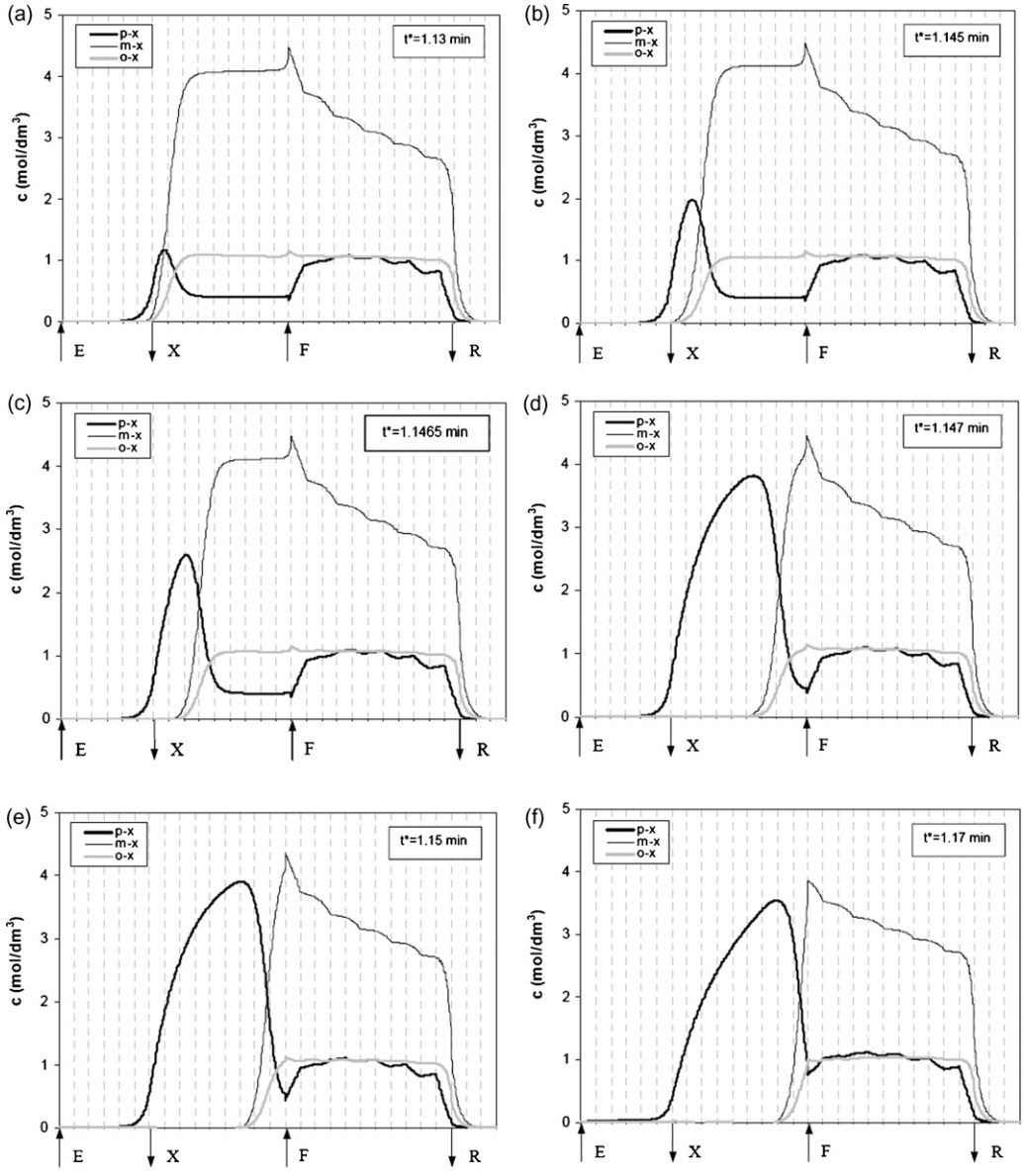

Fig. 8. Steady state concentration profiles in equivalent TMBR with feed B for different switching time: (a) 1.13 min; (b) 1.145 min; (c) 1.1465 min; (d) 1.147 min; (e) 1.15 min; (f) 1.17 min.

domain, respectively. The system of ordinary differential and algebraic equation (ODAEs) was integrated over time using the DASOLV integrator implement in gPROMS. For all simulations was fixed a tolerance value equal to 10^{-5}.

6. Simulation of SMBR for *p*-xylene production

The equivalent TMBR steady state profiles calculated for the operating conditions given in Table 9 for feed A and B, are presented in Fig. 5a and b, respectively.

6.1. Influence of the switching time on SMBR performance

The influence of the switching time on SMBR performance was studied for both type of feed (feed A and B) at 453 K. The SMBR performance considered here are: extract and raffinate purities, *p*-xylene productivity, desorbent consumption and *p*-xylene deviation from reaction equilibrium composition. The desired performances are maximum *p*-xylene productivity, maximum *p*-xylene deviation from the equilibrium and minimum desorbent consumption, within required extract and raffinate purities. The minimum required extract and raffinate purities, in the study of the influence of the switching time, were set on 99% and 95%, respectively.

The effect of the switching time on equivalent TMBR performance in the case of feed A is presented in Fig. 6. The best SMBR performances were obtained for the switching 1.08 min. The *p*-xylene deviation from the equilibrium is high above 1, indicating that *p*-xylene is produced in a considerably higher quantity than that predicted by the isomerization reaction equilibrium. For a switching time higher than 1.08 min the extract and raffinate purities do not change significantly; however, the *p*-xylene pro-

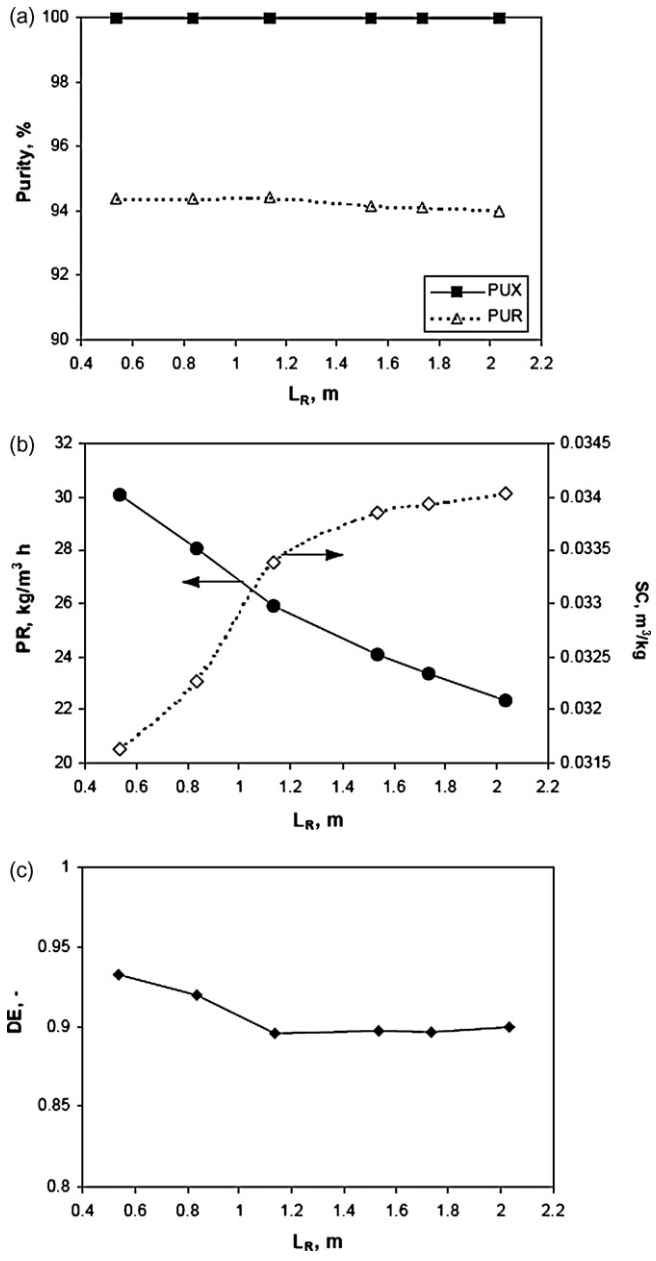

Fig. 9. Influence of the length of the reactor columns on the (a) extract and raffinate purity; (b) *p*-xylene productivity and desorbent consumption; (c) *p*-xylene deviation from equilibrium for feed A.

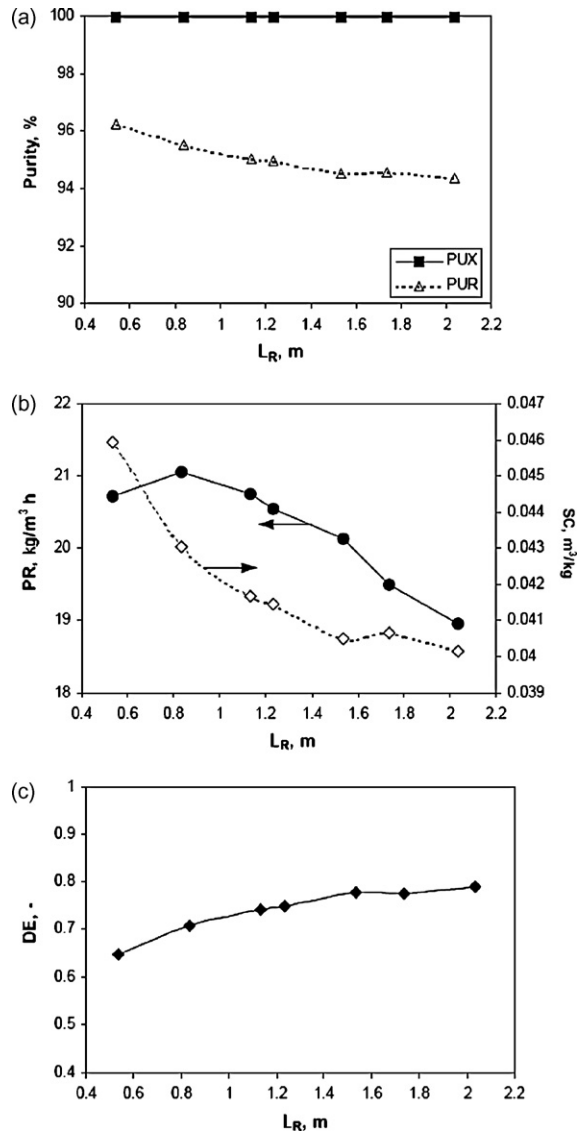

Fig. 10. Influence of the length of the reactor columns on the (a) extract and raffinate purity; (b) *p*-xylene productivity and desorbent consumption; (c) *p*-xylene deviation from equilibrium for feed B.

ductivity and deviation from the equilibrium decrease rapidly and desorbent consumption increase notably. For a switching time lower than 1.08 min the *p*-xylene purity decreases below 99%.

The influence of the switching time on equivalent TMBR performance in the case of feed B is presented in Fig. 7. The best performances were obtained for the switching time 1.147 min. For values of the switching time lower or higher than 1.147 min similar behaviour of the unit performance has been observed as in the case of feed A. When feed of composition B is used the *p*-xylene deviation does not reach 1, which means that the *p*-xylene cannot convert to the equilibrium composition.

The TMBR steady state concentration profiles in the case of feed B for different switching times, starting from $t^* = 1.13$ min until $t^* = 1.17$ min is presented in Fig. 8. It can be observed that for values of the switching time around 1.147 min the distribution of the xylene profiles in zones 2 and 3 could be very different. For example, for switching time 1.145 min the *m*-xylene and *o*-xylene concentration profiles spread in both zones 2 and 3 and for slightly higher value of the switching time (1.147 min) they pass to zone 3, leading to pure *p*-xylene in the extract. Similar behaviour was noticed in the case of feed A, suggesting that from practical reasons is preferable to work with a switching time slightly higher than the optimal value (1.08 min for feed A and 1.147 for feed B), since when operating in these conditions a small disturbance in the switching time could lead to impure *p*-xylene.

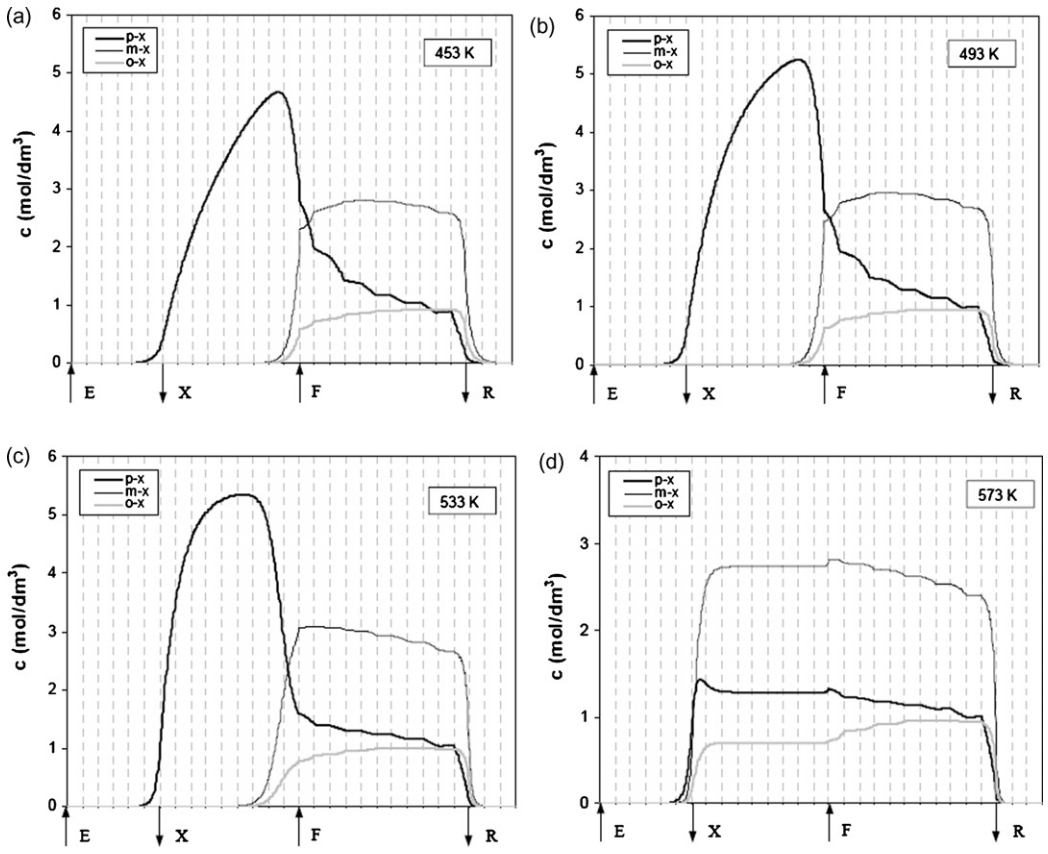

Fig. 11. Steady state concentration profiles in equivalent TMBR with feed A at (a) 453 K; (b) 493 K; (c) 533 K; and (d) 573 K (operating conditions in Table 12).

6.2. *Influence of the reactors length on SMBR performance*

The influence of the reactor column length on the SMBR performance was studied. For this purpose the adsorbent length was keep constant (1.135 m) and the reactor length was changed starting from 0.535 m until 2.035 m. The flow rates in all sections are those presented in Table 9. One should keep in mind that the liquid flow rate in the reactor column for equivalent TMBR is the same as that in the SMBR and for the adsorbent column is calculated as $v_{TMBR} = v_{SMBR} - u_s$. Thus change of the reactors length will not influence the solid and liquid velocity in the TMBR.

The effect of the reactor length on equivalent TMBR performance in the case of feed A is presented in Fig. 9.

The best SMBR performances were obtained for the reactor column length 0.535 m. This has to do with the composition of feed A. The content of *p*-xylene in feed A is above its reaction equilibrium composition. Using shorter reaction columns with the same liquid flow rate in zone 3 leads to shorter residence time and therefore lower conversion of *p*-xylene to *o*-xylene and *m*-xylene, and therefore more *p*-xylene in the extract.

The effect of the reactor length on the TMBR performance in the case of feed B is presented in Fig. 10.

The best performances were obtained for the column length between 0.835 and 1.235 m. In this region the extract purity is constant and raffinate purity decrease slightly with increase of the reactors length. With increase of the reactor columns length the residence time become longer and more *p*-xylene is produced manly from *m*-xylene. Thus, the *p*-xylene deviation from the equilibrium increases with increase of the reactors length. Both *p*-xylene productivity and desorbent consumption decrease with increase of the reactors length and if more importance is given to *p*-xylene productivity reactor columns with 0.835 m length should be used; if more importance is given to the desorbent consumption the reactor columns with 1.235 m should be selected. Otherwise, the reactors length should be chosen according to some economical trade-off between the *p*-xylene productivity and desorbent consumption.

6.3. *Influence of the temperature on SMBR performance*

The influence of the operating temperature on the SMBR performance was studied in a temperature range between 453 and 573 K. The operating conditions were the same for all temperatures. The operating conditions used in the case of feed A and feed B are presented in Table 10. The temperature would influence the adsorption and reaction parameters. The adsorption equilibrium parameters, reaction kinetic constants and reaction equilibrium composition are presented in Tables 5–7, respectively.

The increase of the temperature would lead to lower adsorption capacity of the adsorbent, faster mass transfer and faster xylene isomerization. Also, the number of the moles of xylene introduced in the SMBR for a constant feed flow rate will

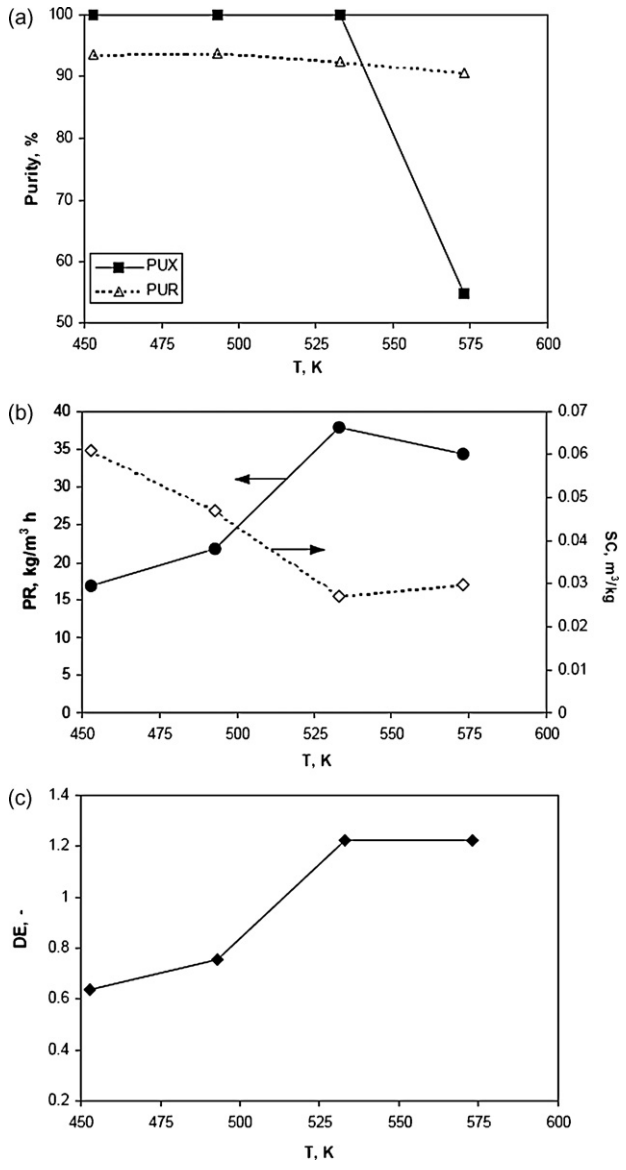

Fig. 12. Influence of the temperature on equivalent TMBR performance for feed A: (a) extract and raffinate purity; (b) *p*-xylene productivity and desorbent consumption; (c) *p*-xylene deviation from equilibrium.

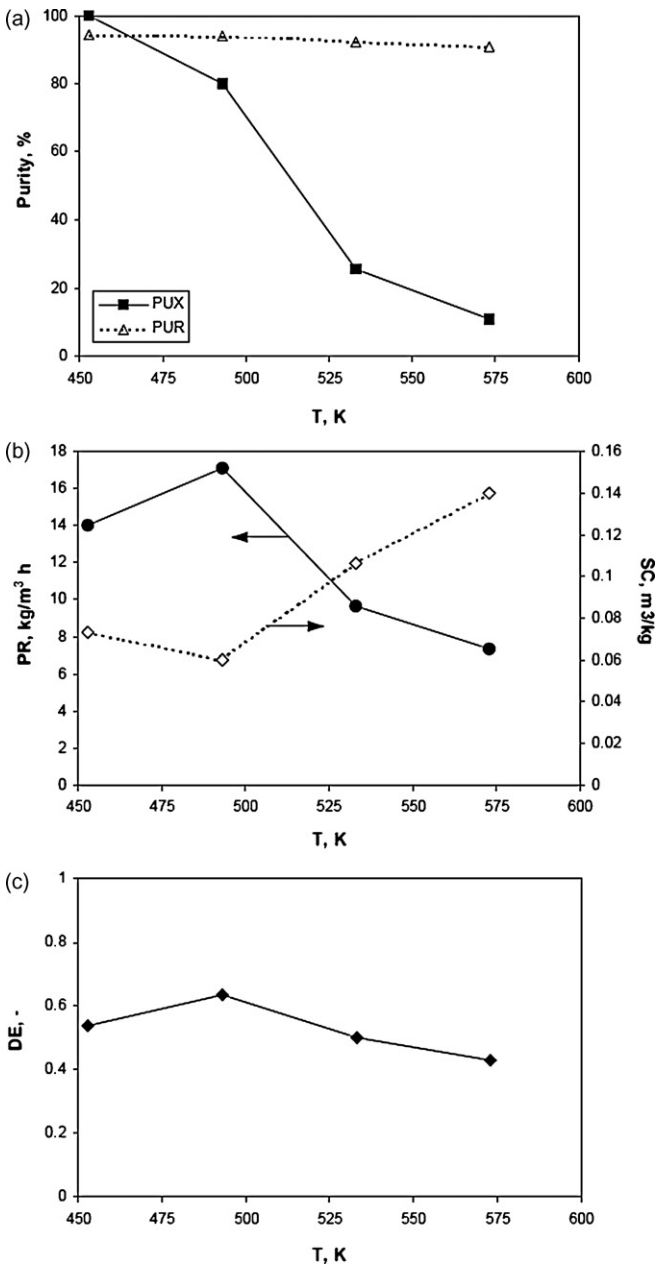

Fig. 13. Influence of the temperature in equivalent TMBR performance for feed B: (a) extract and raffinate purities; (b) *p*-xylene productivity and desorbent consumption; (c) *p*-xylene deviation from equilibrium.

decrease with increase of the temperature. The xylene isomerization equilibrium composition does not change significantly with the increase of the temperature (see Table 7).

In Fig. 11, the TMBR steady state concentration profiles at 453, 493, 533 and 573 K for feed A are presented. The effect of the operating temperature on the TMBR performance in the case of feed A is presented in Fig. 12. For the given operating conditions (Table 11) the best SMBR performance were obtained at 533 K.

Table 10
SMBR operating conditions

SMBR unit geometry	Operating conditions	
	Feed A	Feed B
$L_c = 1.135$ m, $d_c = 4.12$ m, $V_c = 15.13$ m^3, number of columns: 29, configuration: 6-9-(6 + 5)-3	$t^* = 1.15$ min $Q_F^* = 62.29$ m^3/h $Q_X^* = 89.64$ m^3/h $Q_R^* = 204.63$ m^3/h $Q_D^* = 231.99$ m^3/h $Q_I^* = 674.47$ m^3/h	$t^* = 1.15$ min $Q_F^* = 62.29$ m^3/h $Q_X^* = 91.19$ m^3/h $Q_R^* = 203.09$ m^3/h $Q_D^* = 231.99$ m^3/h $Q_I^* = 674.47$ m^3/h

Table 11
The optimum switching time and γ_j at different temperatures in the case of feed A

T (K)	t^* (min)	γ_1	γ_2	γ_3	γ_4
453	1.05	1.106	0.837	1.024	0.411
493	1.09	1.148	0.869	1.063	0.427
533	1.15	1.211	0.917	1.121	0.450
573	1.23	1.295	0.981	1.199	0.482

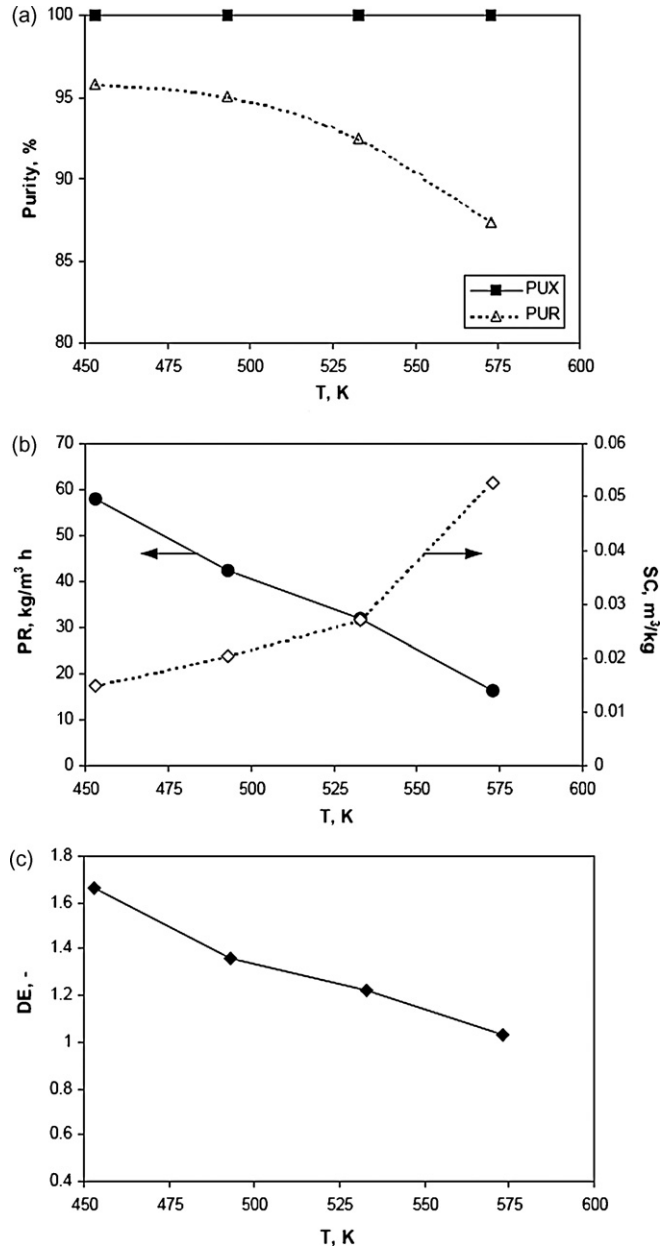

Fig. 14. The TMBR performance at different temperature (a) extract and raffinate purity; (b) *p*-xylene productivity and desorbent consumption; (c) *p*-xylene deviation from equilibrium for optimum switching time and feed A.

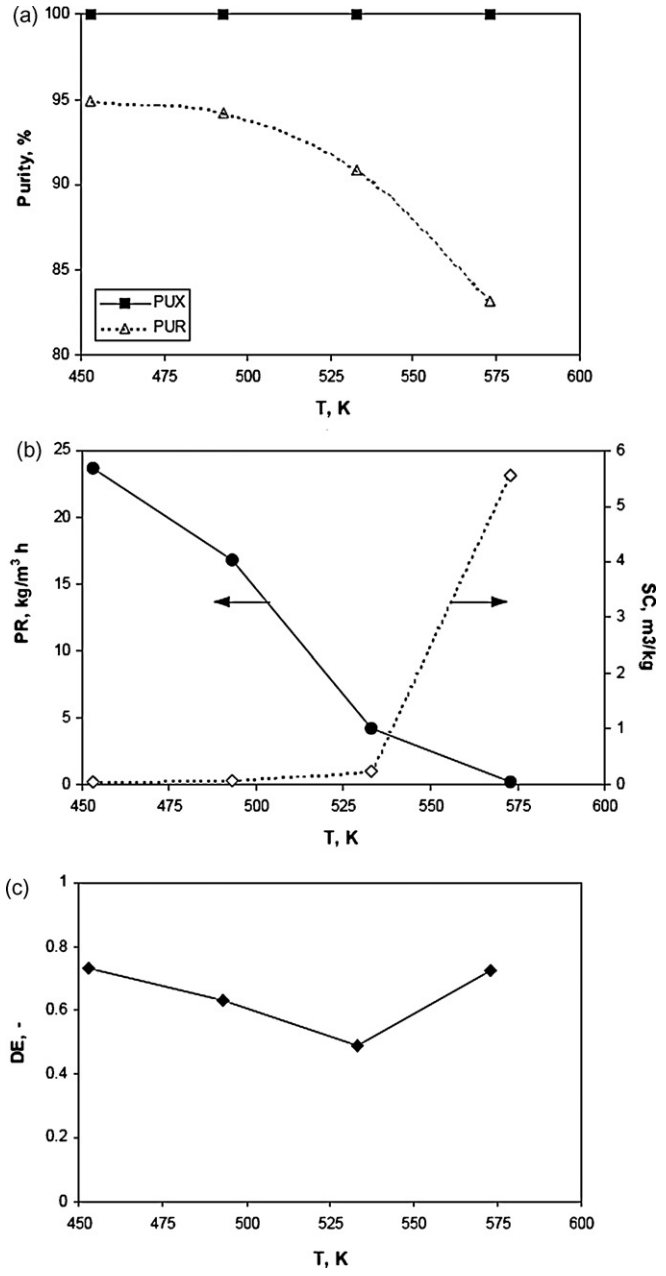

Fig. 15. The TMBR performance at different temperature (a) extract and raffinate purity; (b) *p*-xylene productivity and desorbent consumption; (c) *p*-xylene deviation from equilibrium for optimum switching time and feed B.

At 573 K all xylenes are distributed in zones 2 and 3 and therefore the separation of *p*-xylene from *m*-xylene and *o*-xylene is not possible. Anyhow, this does not mean that the pure *p*-xylene production is not possible at this temperature. The operating conditions should be adjusted for this temperature to yield to *p*-xylene separation.

The effect of the operating temperature on equivalent TMBR performance in the case of feed A is presented in Fig. 12 and in case B on Fig. 13.

For the given operating conditions (Table 11) the best SMBR performance were obtained at 453 K and the separation was not possible above this temperature. Again this does not mean that for another operating condition the best performances would be at the same temperature.

The comparison of SMBR performance at different temperatures should be done by comparison of SMBR optimised performance at each temperature for a given feed flow rate, or more precisely for a given number of moles of xylenes introduced in the SMBR. The optimisation of a given SMBR with previously defined unit configuration considers determination of the switching time and flow rates in each zone that lead to best performance. In this particular case the optimum SMBR performance means the desired extract and raffinate purities, with maximum *p*-xylene deviation from the equilibrium and maximum *p*-xylene productivity and in same time minimum

Table 12
The optimum switching time and γ_j at different temperatures in the case of feed B

T (K)	t^* (min)	γ_1	γ_2	γ_3	γ_4
453	1.13	1.190	0.409	0.578	0.825
493	1.16	1.221	0.414	0.586	0.840
533	1.22	1.284	0.423	0.602	0.869
573	1.35	1.421	0.442	0.633	0.930

desorbent consumption. The complete SMBR optimisation is a multiobjective problem. At this point just optimisation of the switching time for a fixed TMBR flow rates, corresponding to those presented in Table 10, is considered. The switching time was optimised for each temperature in the case of feed A and B. Optimisation of the switching time at each temperature considers determination of the switching time that leads to maximum *p*-xylene productivity, within minimum 99% extract purity. The optimum switching times and corresponding liquid/solid interstitial velocities ratio, γ_j, ($\gamma_j = v_j/u_s$) at different temperatures for equivalent TMBR fed with feed of type A and B are presented in Tables 11 and 12, respectively.

The TMBR performance at the optimum switching time at each temperature for feed A and B, are presented in Figs. 14 and 15, respectively. In both case, feed A and feed B, the best performances were obtained at 453 K. The optimum temperatures for feed of type A and B obtained by the optimisation of the switching time at each temperature is different from the ones determined before. Also, the TMBR performances were significantly improved. The final decision of the operating temperature should be make just after optimisation of the SMBR unit design and operation, taking into consideration the all decision parameters as the number of absorbers and reactors, their geometry, adsorbent and catalyst particle size, the flow rates in each zone, switching time and operating temperature.

7. Conclusions

The novel SMBR application for *p*-xylene production by isomerization of xylene mixture free of ethylbenzene is proposed. The SMBR unit consists of separated reactor and adsorption columns operating in liquid phase at temperature between 453 and 573 K. The SMBR configuration contains reactors just in zone 3. There are five reactors and six adsorbers in zone 3, which starts with adsorber and finishes with an adsorber. The feed enters first in the adsorber; moreover, the reactors switch in direction of the liquid flow together with the inlet and outlet streams; therefore they are fixed relatively to the inlet and outlet streams.

Two types of xylenes feed were considered: feed A, where the *p*-xylene composition is above its reaction equilibrium composition and feed B, where the *p*-xylene composition is below its equilibrium composition. The SMBR unit was modelled using the equivalent TMBR strategy and its operation was studied through simulation. The influence of the switching time, reactors length and operating temperature on SMBR performances was evaluated. The SMBR performances were the extract and raffinate purities, *p*-xylene productivity, desorbent consumption and *p*-xylene deviation from equilibrium. The performance is very sensitive to small changes of the switching time especially for switching times that leads to best SMBR performance. For both types of xylene feed is better to use shorter reactors (0.535 m in the case of feed A and 0.835 m in the case of feed B) and to work on lower temperature (453 K for feed A and B). When *p*-xylene in the feed is above its reaction equilibrium composition the values of the *p*-xylene deviation from equilibrium could reach value of 1.75, otherwise the *p*-xylene deviation from equilibrium is below 1.

Acknowledgement

Financial support through the project POCTI/EQU/44515/2002 from FCT "Fundação para a Ciência e a Tecnologia", Minister for Science, Technology and Higher Education of Portugal is gratefully acknowledged.

Appendix A. Modelling and simulation of fixed bed catalytic reactor for xylenes isomerization

In the work of Cappellazzo et al. [56] simple mass balance equations are used to calculate the xylene concentration at the outlet of the catalytic reactor. In this section a more detailed fixed bed catalytic reactor model was developed. The model includes external mass transfer resistance, axial dispersion, diffusion inside catalyst pellet, coupled with chemical reaction within an individual catalyst pellet. Model equations are:

Bulk fluid mass balance for component i ($i = 1, 2, 3$ (ox, mx, px))

$$D_L \frac{\partial^2 c_i}{\partial z^2} = v\frac{\partial c_i}{\partial z} + \frac{\partial c_i}{\partial t} + \frac{1-\varepsilon}{\varepsilon} k_{fi}(c_i - c_{pi}|_{r_p}) \tag{A1}$$

with the boundary conditions:

$$z = 0: \quad D_L \frac{\partial c_i}{\partial z} = v(c_i - c_{iF}) \tag{A2a}$$

$$z = L: \quad \frac{\partial c_i}{\partial z} = 0 \tag{A2b}$$

Particle mass balance for component i

$$D_{ei}\left(\frac{\partial^2 c_{pi}}{\partial r^2} + \frac{2}{r}\frac{\partial c_{pi}}{\partial r}\right) = \varepsilon_p \frac{\partial c_i}{\partial t} + \rho_{p(cat)} R_i \tag{A3}$$

with the boundary conditions

$$r = r_p: \quad D_{ei}\frac{\partial c_{pi}}{\partial r} = k_{fi}(c_i - c_{pi}|_{r_p}) \tag{A4a}$$

$$r = 0: \quad \frac{\partial c_{pi}}{\partial r} = 0 \tag{A4b}$$

Reaction rates of consumption of o-x, m-x and p-x are R1, R2 and R3 given by Eqs. (1)–(3).

Initial conditions are: $t = 0$: $c_i = 0$, $c_{pi} = 0$.

In the above equations c_i and c_{pi} are the liquid bulk and pore concentrations of component i, ε and ε_p are the bed and catalyst

porosity, $\rho_{p(cat)}$ is the catalyst apparent density, k_{fi} is the film mass transfer coefficient of component i, D_{ei} is the effective pore diffusion coefficient of component i, D_L and v are the axial dispersion coefficient and the interstitial velocity, respectively, r_p is the particle radius, t is the time variable and z is the axial coordinate.

The model parameters [56] used in the simulations are presented in Table A1. The fixed bed reactor was simulated for five different LWHSV (liquid weight hourly space velocities) at temperature 553 K. The same feed composition 27.5 wt% *o*-xylene, 60.4 wt% *m*-xylene and 12.1 wt% *p*-xylene was used in all simulation runs.

In the work of Cappellazzo et al. [56] the xylenes concentration histories at the outlet of the catalytic reactor are not reported. The reactor concentration histories calculated with the proposed model for different LWHSV are presented in Fig. A1.

Table A1
Fixed bed reactor model parameters

r_p (m)	1×10^{-3}
d_c (m)	3.1×10^{-2}
L (m)	3.3
D_e (m^2/s)	1.61×10^{-9}
LWHSV $\times 10^3$ (s^{-1})	5.556; 2.778; 1.306; 0.694; 0.472
T (K)	553
ε_b	0.4
ε_p	0.4
ρ_ρ (kg/m^3)	930
ρ_l (kg/m^3)	900
D_L (m^2/s)	4.72×10^{-9}
Feed composition (wt%)	$o = 27.5$, $m = 60.4$, $p = 12.1$

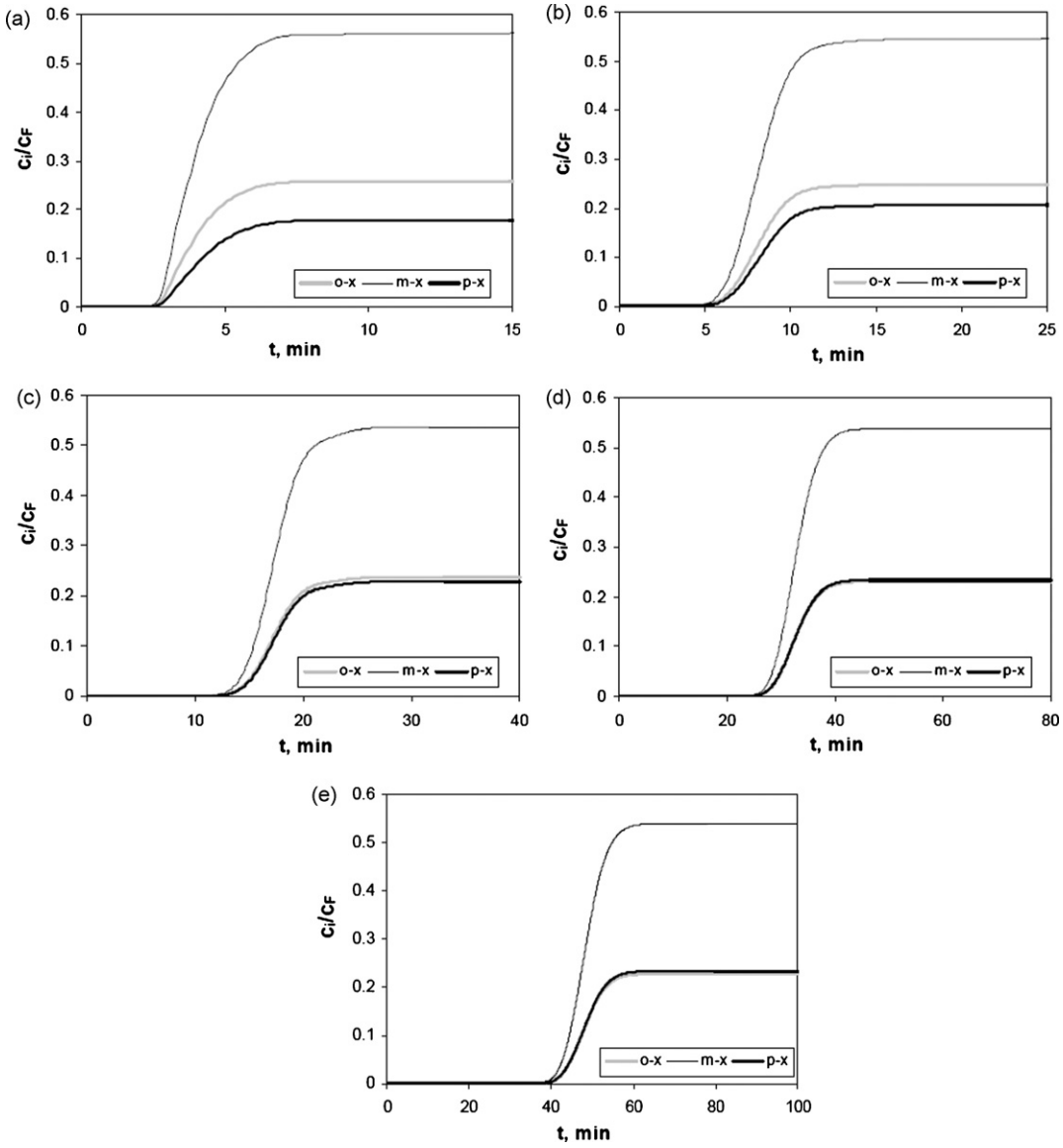

Fig. A1. Concentration histories at the outlet of the fixed bed catalytic reactor: (a) 5.56×10^{-3} s^{-1}; (b) 2.78×10^{-3} s^{-1}; (c) 1.31×10^{-3} s^{-1}; (d) 0.694×10^{-3} s^{-1}; (e) 0.472×10^{-3} s^{-1} LWHSV.

Table A2
Comparison of the steady state fixed bed catalytic reactor outlet composition calculated by Cappellazzo et al. [56] and in this work

LWHSV (h^{-1})	Cappellazzo et al. [56]			This work		
	m-x (wt%)	*p*-x (wt%)	*o*-x (wt%)	*m*-x (wt%)	*p*-x (wt%)	*o*-x (wt%)
20	56.5	17.5	26.0	56.3	17.9	25.9
10	54.7	20.4	24.9	54.5	20.6	24.8
4.7	53.5	22.9	23.6	53.6	22.8	23.6
2.5	53.5	23.7	22.8	53.8	23.3	23.0
1.7	53.7	23.8	22.5	53.9	23.3	22.8

In absence of concentration histories for comparison, the steady state outlet composition calculated by Cappellazzo et al. [56] and the proposed model, for different LWHSV, were compared (see Table A2).

As shown in Table A2, the xylene steady state outlet composition calculated with both models is very close. The disadvantage of the detailed models is that normally they require longer computation time when applied for the simulation of more complex systems, as for example the SMBR. Therefore the above model was simplified by coupling the external (film mass transfer) and internal mass transfer (pore diffusion) in a single mass transfer step. The mass transfer from the bulk liquid phase to the zeolite particle was presented with a Linear Driving Force (LDF) model and total mass transfer coefficient [62]:

The model equations for the simplified model are now:

Bulk fluid mass balance for component i ($i = 1, 2, 3$ (ox, mx, px)):

$$D_L \frac{\partial^2 c_i}{\partial z^2} = v\frac{\partial c_i}{\partial z} + \frac{\partial c_i}{\partial t} + \frac{1-\varepsilon}{\varepsilon} k_{Li}(c_i - \bar{c}_{pi}) \tag{A5}$$

with boundary conditions given by Eqs. (A4a) and (A4b).

Particle mass balance for component i

$$\frac{3}{r_p} k_{Li}(c_i - \bar{c}_{pi}) = \varepsilon_p \frac{\partial \bar{c}_{pi}}{\partial t} + \rho_{p(cat)} R_i \tag{A6}$$

The reaction rates for o-x, m-x and p-x are given by Eqs. (1)–(3) but the species concentrations are $\bar{c}_{p,ox}$, $\bar{c}_{p,mx}$ and $\bar{c}_{p,px}$.

The initial conditions are: $t = 0$, $c_i = 0$ and $\bar{c}_{pi} = 0$. Here $\bar{c}_{pi}$ is the average pore concentration of species i.

The k_{Li} is the global mass transfer coefficient of component i

$$\frac{1}{K_{Li}} = \frac{1}{k_f} + \frac{1}{\varepsilon_p k_p} \tag{A7}$$

The mean value estimated of the internal mass transfer coefficient was calculated as [65] $k_i = (5D_m/\tau)/r_p$.

The external mass transfer coefficient was estimated by the Wilson and Geankoplis correlation [66], $Sh_p = 1.09/\varepsilon(Re_p Sc)^{0.33}$ $0.0015 < Re_p < 55$ where Sh_p and Re_p are, respectively, the Sherwood and Reynolds numbers, relative to particle and Sc is the Schmidt number:

$$Sh_p = \frac{k_f d_p}{D_m}, \qquad Re_p = \frac{\rho d_p v}{\mu}, \qquad Sc = \frac{\mu}{\rho D_m}$$

The concentration history at the outlet of the reactor for $5.56 \times 10^{-3}\ s^{-1}$ LWHSV was simulated using the lumped model Eqs. (A5)–(A7) and compared with those calculated by the detail model Eqs. (A1)–(A4) (see Fig. A2). Both models give identical prediction of the concentration profiles.

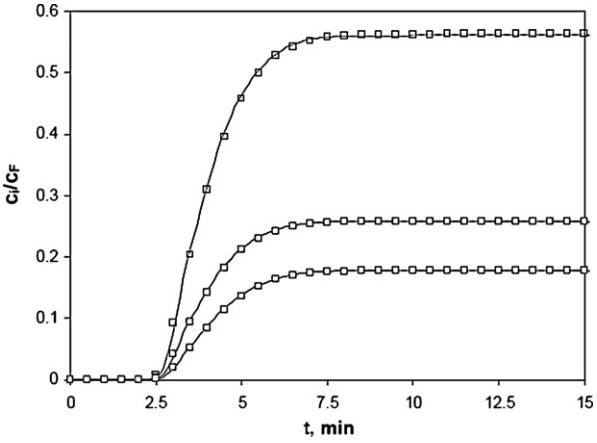

Fig. A2. Comparison of the concentration history at the outlet of the column calculated by (—) the film-pore diffusion model and (□) lumped model for liquid weight hourly space velocity (LWHSV) of $5.56 \times 10^{-3}\ s^{-1}$.

References

[1] F.M. Dautzenberg, M. Mukherjee, Chem. Eng. Sci. 56 (2001) 251–267.
[2] A.L. Paiva, F.X. Malcata, Biopro. Eng. 22 (2000) 149–158.
[3] A.L. Paiva, F.X. Malcata, Chem. Eng. Sci. 55 (2000) 589–599.
[4] A.L. Paiva, D. van Rossum, F.X. Malcata, Chem. Eng. Sci. 54 (1999) 1825–1836.
[5] I. Yongsunthon, E. Alpay, Chem. Eng. Sci. 55 (2000) 5643–5656.
[6] M.P. Elsner, M. Menge, C. Muller, D.W. Agar, Catal. Today 79 (2003) 487–494.
[7] H.J. Gorissen, Chem. Eng. Sci. 58 (2003) 809–814.
[8] R.F. Zabransky, R.F. Anderson, Simulated Moving Bed Alkylation Process, 1977.
[9] K. Hashimoto, S. Adachi, H. Noujima, Y. Ueda, Biotechnol. Bioeng. 25 (1983) 2371–2393.
[10] M. Mazzotti, A. Kruglov, B. Neri, D. Gelosa, M. Morbidelli, in: Proceedings of the 1996 14th International Symposium on Chemical Reaction Engineering: From Fundamentals to Commercials to Commercial Plants and Products, ISCRE 14, Part A, May 5–8, 1996, Chem. Eng. Sci. 51 (1996) 1827–1836.
[11] M. Kawase, Y. Inoue, T. Araki, K. Hashimoto, Catal. Today 48 (1999) 199–209.
[12] M.T. Shieh, P.E. Barker, J. Chem. Technol. Biotechnol. 63 (1995) 125–134.
[13] A.L.Y. Tonkovich, R.W. Carr, in: Proceedings of the 13th International Symposium on Chemical Reaction Engineering, Part A, September 25–28, Chem. Eng. Sci. 49 (1994) 4647–4656.
[14] Z.Y. Zhang, K. Hidajat, A.K. Ray, Ind. Eng. Chem. Res. 41 (2002) 3213–3232.

[15] D.C.S. Azevedo, A.E. Rodrigues, Chem. Eng. J. 82 (2001) 95–107.
[16] J. Fricke, M. Meurer, H. Schmidt-Traub, Chem. Eng. Tech. 22 (1999) 835–839.
[17] J. Fricke, H. Schmidt-Traub, Chem. Eng. Proc. 42 (2003) 237–248.
[18] M. Migliorini, A. Gentilini, M. Mazzotti, M. Morbidelli, Ind. Eng. Chem. Res. 38 (1999) 2400–2410.
[19] M. Minceva, V.M.T. Silva, A.E. Rodrigues, Ind. Eng. Chem. Res. 44 (2005) 5246–5255.
[20] V.M.T.M. Silva, Diethylacetal Synthesis in Simulated Moving Bed Reactor, University of Porto, Porto, 2003.
[21] G. Strohlein, M. Mazzotti, M. Morbidelli, Chem. Eng. Sci. 60 (2005) 1525–1533.
[22] H.J. Subramani, K. Hidajat, A.K. Ray, Comput. Chem Eng. 27 (2003) 1883–1901.
[23] Y. Zhang, K. Hidajat, A.K. Ray, BioChem. Eng. J. 21 (2004) 111–121.
[24] G. Dünnebier, J. Fricke, K.-U. Klatt, Ind. Eng. Chem. Res. 39 (2000).
[25] C. Migliorini, M. Fillinger, M. Mazzotti, M. Morbidelli, in: Proceedings of the 1998 15th International Symposium on Chemical Reaction Engineering, ISCRE 15, September 13–16, Chem. Eng. Sci. 54 (1999) 2475–2480.
[26] M. Minceva, A.E. Rodrigues, AIChE J. 51 (2005) 2737–2751.
[27] G. Biressi, O. Ludemann-Hombourger, M. Mazzotti, R.-M. Nicoud, M. Morbidelli, J. Chromatogr. A 876 (2000) 3–15.
[28] A.S. Kurup, H.J. Subramani, K. Hidajat, A.K. Ray, Chem. Eng. J. 108 (2005) 19–33.
[29] H.J. Subramani, Z. Zhang, K. Hidajat, A.K. Ray, Can. J. Chem. Eng. 82 (2004) 590–598.
[30] P.E. Barker, G. Ganetsos, J. Ajongwen, A. Akintoye, Chem. Eng. J. BioChem. Eng. J. 50 (1992) B23–B28.
[31] C.B. Ching, Z.P. Lu, Ind. Eng. Chem. Res. 36 (1997) 152–159.
[32] M. Meurer, U. Altenhöner, J. Strube, A. Untiedt, H. Schmidt-Traub, Starch 48 (1996) 452–457.
[33] G. Ganetsos, P.E. Barker, J.N. Ajongwen, Batch and continuous chromatographic systems as combined bioreactor-separators, in: G. Ganetsos, P.E. Barker (Eds.), Preparative and Production Scale Chromatography, Marcel Dekker, New York, 1993, pp. 375–394.
[34] K. Hashimoto, S. Adachi, Y. Shirai, Development of new bioreactors of a simulated moving-bed type, in: G. Ganetsos, P.E. Barker (Eds.), Preparative and Production Scale Chromatography, Marcel Dekker, New York, 1993, pp. 395–419.
[35] A.K. Ray, R.W. Carr, R. Aris, Chem. Eng. Sci. 49 (1994) 469–480.
[36] A. Kruglov, Chem. Eng. Sci. 49 (1994) 4699–4716.
[37] M.C. Bjorklund, R.W. Carr, Ind. Eng. Chem. Res. 41 (2002) 6528–6536.
[38] M.C. Bjorklund, A.V. Kruglov, R.W. Carr, Ind. Eng. Chem. Res. 40 (2001) 2236–2242.
[39] A.L.Y. Tonkovich, R.W. Carr, in: Proceedings of the 13th International Symposium on Chemical Reaction Engineering, Part A, September 25–28, Chem. Eng. Sci. 49 (1994) 4657–4665.
[40] M.T. Shieh, P.E. Barker, J. Chem. Tech. Biotechnol. 66 (1996) 265–278.
[41] M. Kawase, T.B. Suzuki, K. Inoue, K. Yoshimoto, K. Hashimoto, in: Proceedings of the 14th International Symposium on Chemical Reaction Engineering, Part B, May 5–8, Chem. Eng. Sci. 51 (1996) 2971–2976.
[42] M. Kawase, A. Pilgrim, T. Araki, K. Hashimoto, Chem. Eng. Sci. 56 (2001) 453–458.
[43] F. Lode, M. Houmard, C. Migliorini, M. Mazzotti, M. Morbidelli, Chem. Eng. Sci. 56 (2001) 269–291.
[44] F. Lode, M. Mazzotti, M. Morbidelli, AIChE J. 49 (2003) 977–990.
[45] W.F. Yu, K. Hidajat, A.K. Ray, Ind. Eng. Chem. Res. 42 (2003) 6743–6754.
[46] Z. Zhang, K. Hidajat, A.K. Ray, Ind. Eng. Chem. Res. 40 (2001) 5305–5316.
[47] V. Silva, A.E. Rodrigues, AIChE J. 51 (2005) 2752–2768.
[48] R. Baur, R. Krishna, Chem. Eng. J. 109 (2005) 107–113.
[49] G. Strohlein, Y. Assunção, N. Dube, A. Bardow, M. Mazzotti, M. Morbidelli, Chem. Eng. Sci. 61 (2006) 5296–5306.
[50] D. Fissore, D.G. Tejedor, A.A. Barresi, AIChE J. 52 (2006) 3146–3154.
[51] H.H. John, H.D. Neubauer, P. Birke, Catal. Today 49 (1999) 211–220.
[52] A. Iliyas, S. Al-Khattaf, Appl. Catal. A: Gen. 269 (2004) 225–236.
[53] A. Iliyas, S. Al-Klattaf, Ind. Eng. Chem. Res. 43 (2004) 1349–1358.
[54] Y.G. Li, H. Jun, Appl. Catal. A: Gen. 142 (1996) 123–137.
[55] L.B. Young, S.A. Butter, W.W. Kaeding, J. Catal. 76 (1982) 418–432.
[56] O. Cappellazzo, G. Cao, G. Messina, M. Morbidelli, Ind. Eng. Chem. Res. 30 (1991) 2280–2287.
[57] A. Cortes, A. Corma, J. Catal. 51 (1978) 338–344.
[58] A. Corma, A. Cortes, Ind. Eng. Chem. Proc. Des. Dev. 19 (1980) 263–267.
[59] K.H. Robschlager, E.G. Christoffel, Can. J. Chem. Eng. 58 (1980) 517–520.
[60] J.R. Hopper, Ds. Shigemur, AIChE J. 19 (1973) 1025–1032.
[61] G.H. Norman, D.S. Shigemura, J.R. Hopper, Ind. Eng. Chem. Prod. Res. Dev. 15 (1976) 41–45.
[62] E. Santacesaria, M. Morbidelli, P. Danise, M. Mercenari, S. Carra, Ind. Eng. Chem. Proc. Des. Dev. 21 (1982) 440–445.
[63] M. Minceva, A.E. Rodrigues, Chem. Eng. Res. Des. 82 (2004) 667–681.
[64] S.B. Neves, Modeling of Adsorption Fixed-Bed in Liquid–Solid Systems, Universidade Federal da Bahia, Brazil, 1995.
[65] E. Glueckauf, Trans. Faraday Soc. 51 (1955) 1540–1551.
[66] D.M. Ruthven, Principles of Adsorption and Adsorption Processes, Wiley, New York, 1984, p. 464.